QUANTIFYING GEOMORPHIC CHANGE TO A POINT BAR IN RESPONSE TO HIGH FLOW EVENTS USING TERRESTRIAL LIDAR, WHITE CLAY CREEK, DE

by

Michael J. Orefice

A thesis submitted to the Faculty of the University of Delaware in partial fulfillment of the requirements for the degree of Master of Science in Geology

Summer 2015

QUANTIFYING GEOMORPHIC CHANGE TO A POINT BAR IN RESPONSE TO HIGH FLOW EVENTS USING TERRESTRIAL LIDAR, WHITE CLAY CREEK, DE

by

Michael J. Orefice

Approved: ____

James E. Pizzuto, Ph.D.
Professor in charge of thesis on behalf of the Advisory Committee

Approved: ____

Neil C. Sturchio, Ph.D.
Chair of the Department of Geological Sciences

Approved: ____

Nancy M. Targett, Ph.D.
Dean of the College of Earth, Ocean, and Environment

Approved: ____

James G. Richards, Ph.D.
Vice Provost for Graduate and Professional Education

ACKNOWLEDGMENTS

I would like to thank my advisors Dr. Jim Pizzuto and Dr. Michael O'Neal for their guidance throughout my time at the University of Delaware. Without their assistance, this research would not have been possible. Additionally, I would like to thank Dr. Jessica Mitchell for being part of my committee and for her guidance on working with LiDAR point clouds. I am grateful for everything that I have learned from my committee and for all of the suggestions they provided throughout the process.

I would like to express my appreciation to the members of my lab group: Tobi Ackerman, Adam Pearson, Bridget O'Neill, Meg Christie, and Dale Lambert. Throughout my time at the University of Delaware, they provided valuable feedback and direction in regards to methods and figures. Furthermore, I would like to thank Corey Hovanec and Dan Hubacz for assisting with much of the fieldwork and LiDAR data processing needed for this thesis. Acquiring the LiDAR data required long days in the field, and both were always willing to help.

Finally, I would like to thank all of my family and friends who provided support and feedback throughout the process.

TABLE OF CONTENTS

LIST OF TABLES

LIST OF FIGURES

ABSTRACT

Light Detection And Ranging (LiDAR) data can be used to accurately model three- dimensional surfaces for quantifying fluvial erosion and deposition. Terrestrial LiDAR is typically used for monitoring banks, but can be used for monitoring planar forms such as point bars. Point bars are topographic features that form on the convex bank of a meander. While point bars are considered to be formed by depositional processes, they display features such as chute channels and scour holes that suggest that erosion, due to high flow events, may significantly influence point bar evolution. Through the use of Terrestrial Laser Scanning (TLS), we observed how a point bar on the White Clay Creek near Newark, Delaware, responded to a flood event with a return period of 6.1 years, and to multiple small events over a 1 year period with return periods between 1.00 and 1.25 years. Scans of the point bar were completed on April 11, 2014, May 8, 2014, and April 16, 2015. Scans were referenced to a common coordinate system, scan data representing vegetation points were removed, and three 0.1 m x 0.1 m gridded Digital Elevation Models (DEMs) were created from the remaining data. DEMs of Difference (DoDs) were calculated by subtracting the cell values in subsequent DEMs and by thresholding out positional and surface roughness errors. The 6.1 year flood that occurred between the April 11, 2014 scan and the May 8, 2014 scan resulted in 88.53 m^3 of erosion and 39.12 m^3 of deposition. The net volumetric change was -49.40 m^3 over an area of 631.72 m^2. The smaller events that occurred between the May 8, 2014 scan and the April 16, 2015 scan resulted in 13.33 m^3 of erosion and 53.46 m^3 of deposition. The net volumetric change was

40.13 m^3 over an area of 620.74 m^2. Our results suggest that 1) sediment deposited on point bars is eroded frequently by flood events; and 2) TLS can provide useful estimates of erosion and deposition. Although our results are for a short period, longer datasets can be used to calculate sediment residence times for point bar deposits. Additionally, we can gain a better understanding of how point bar deposits are preserved in the geologic record. This information is useful for creating accurate sediment budgets, remediating contamination issues, and interpreting geologic history.

Chapter 1

INTRODUCTION

During sediment transport, particles travel downstream and are stored in sediment sinks such as point bars, floodplains, and fine-grained channel margin (FGCM) deposits (Skalak and Pizzuto, 2010). The average amount of time that sediment remains stored within a sediment sink is referred to as residence time or average transit time (Eriksson, 1971; Bolin and Rodhe, 1973). Recent studies have calculated residence time for FGCM deposits (Skalak and Pizzuto, 2010) and laterally accreted floodplain deposits (Bradley and Tucker, 2013), but residence time for sediment deposited on a point bar has yet to be calculated. Contaminants move downstream attached to fine-grained particles and can remain stored for many years. With an increase in the concern for how long it takes contaminants to move through a watershed, it is important to quantify the amount of sediment that is transferred in and out of fluvial sediment sinks.

Point bars are topographic features that form along the convex bank of a meander bend. As erosion takes place on the concave bank, deposition occurs on the convex bank, which leads to a lateral shift of the channel (Brierley and Fryirs, 2005). When the channel shifts, the point bar gets extended and old point bar deposits get buried by vertical accretion. Point bar deposits make up a large portion (60% - 90%) of overall floodplain deposits, which makes them an important, and perhaps overlooked, part of the fluvial system (Wolman and Leopold, 1957; Fryirs and Brierley, 2013). Previous studies have monitored point bar migration using cross-sectional surveys (Wolman and Leopold, 1957; Moody and Meade, 2014), while others have used Terrestrial Laser Scanning (TLS) techniques such as LiDAR (Light Detection and Ranging) to measure erosion and deposition associated with fluvial landforms (O'Neal and Pizzuto, 2010; Kasvi et al., 2012; Picco et al., 2013; Starek et al., 2013; Kuo et al., 2014).

While point bars are considered to be depositional features, they display morphological features such as chute channels and scour holes that suggest erosion, due to high flow events, plays a significant role in their evolution (Brierley and Fryirs, 2005; Moody and Meade, 2014). This erosion has not been monitored extensively, and it is important for at least two reasons. First, it helps to explain how certain features develop on a point bar, which in turn, allows us to better interpret the geologic record. Second, if sediment is eroded frequently by small to moderate size flow events, than residence time of active point bar deposits will be short.

This thesis presents high-resolution Digital Elevation Models (DEMs), and DEMs of Difference (DoDs) created from repeat LiDAR scans of a point bar on the White Clay Creek near Newark, Delaware. By observing the DoDs, as well as cross sections created form the DEMs, we investigate the effects that flood events of varying magnitudes have on the evolution of a point bar. The research presented here adds to the existing knowledge of the origin of point bar morphology. Additionally, the TLS scans provide a more accurate representation of the point bar surface than traditional surveys, allowing improved estimates of erosion and deposition.

Chapter 2

BACKGROUND

2.1 Point Bars

Wolman and Leopold (1957) and Nanson and Croke (1992) describe lateral point bar accretion and overbank vertical accretion as the two main ways that floodplains form. Lateral point bar accretion occurs when sediment is deposited on the convex (inside) bank of a meander bend. As the channel migrates laterally, new point bar deposits extend the floodplain while old point bar deposits become buried by overbank deposits. Overbank vertical accretion occurs during flood events and results in fine-grained deposition above laterally accreted point bar deposits. This thesis is particularly concerned with point bar deposits, and a review of the literature provides insight as to their formation and characteristics.

Wolman and Leopold (1957) describe a point bar of Watts Branch in Maryland as having sediment that is not necessarily of greater size than what is in the channel. The stratigraphy of the point bar deposits consists of interbedded sand and gravel with some clay. This stratigraphy can make it difficult to discern the fine-grained overbank deposits from the point bar deposits. Furthermore, Wolman and Leopold (1957) conclude that deposits on the point bar are, for the most part, lower in elevation than the rest of the floodplain, but that their elevations encompass all values from the water surface to the flat upper floodplain surface.

Nanson (1980) describes point bar deposits of the Beatton River in Canada as being largely unvegetated and having sediment ranging in size from silt to gravel. They form first through the development of a point bar platform, which is relatively flat and consists of coarse-grained material. A ridge (scroll bar) then forms on the surface and ridge and swale topography is established. The scroll bar continues to grow until it is built up to the elevation of the rest of the floodplain and becomes vegetated. It is then referred to as a floodplain ridge (Nanson, 1980).

The point bar monitored in this thesis has characteristics similar to those described by Nanson (1980). It is largely un-vegetated compared to the rest of the floodplain and consists of sediment ranging in size from mud to cobbles. A large scroll bar has formed, and it is separated from the vegetated upper floodplain surface by a chute channel.

Depositional and erosional morphological features such as scroll bars, ridges, chute channels, and lee dunes can form on point bars (Figure 2.1). Scroll bars are elongated depositional ridges that may become vegetated (Nanson, 1980; Brierley and Fryirs, 2005). Ridges and chute channels are features that form during high flow. Ridges fine downstream and may form due to sediment dropping from suspension when water flows around vegetation. Chute channels are areas of lower elevation on the point bar where water is directed during high flow. While thought to be erosional features, there is evidence to suggest that chute channels may form through either erosional or depositional processes (Brierley and Fryirs, 2005; Ghinassi, 2011; Moody and Meade, 2014). Moody and Meade (2008) describe a lee dune as an elongated deposit of sand sized sediment that forms downstream of an object such as a tree or rock during overbank flow.

Nanson (1980), Allmendinger (2004), and Moody and Meade (2014) describe a point bar platform as a flat deposit of sand and gravel that encourages deposition and lateral movement of point bars. Platforms are the basal surface of point bar deposits; the aforementioned features form on top of them. Platforms are short-lived when compared with the lifespan of the point bar. Once the platform develops a convex shape, it further promotes deposition and becomes more resistant to erosion.

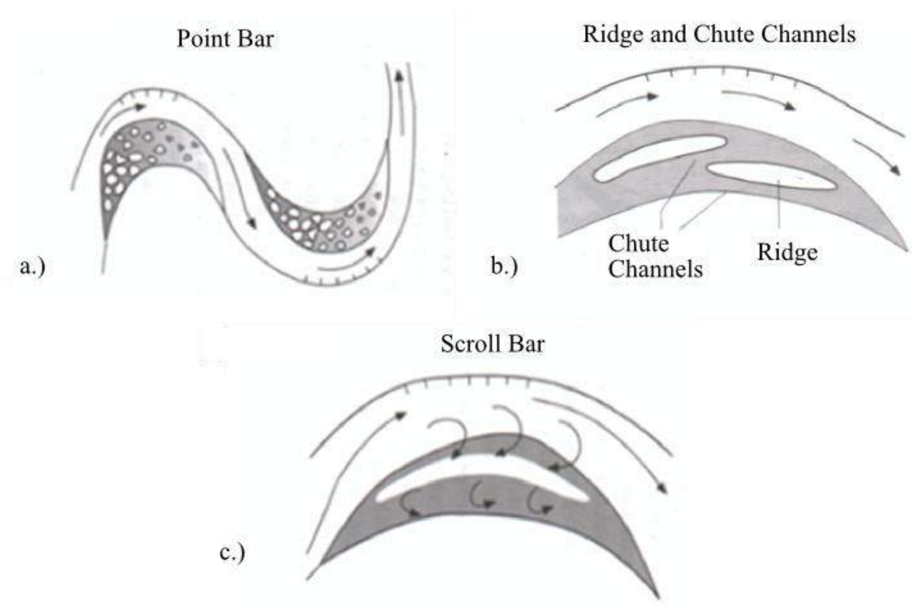

Figure 2.1. a.) Typical point bar with coarse material deposited upstream. b.) Ridge and chute channels that form on the point bar platform. c.) Location of a scroll bar on the point bar platform. (Brierley and Fryirs, 2005)

Allmendinger (2004) created a conceptual model for convex-bank floodplain development in the mid-Atlantic region that describes point bars as having a platform and hummocks. Allmendinger (2004) defines a convex-bank floodplain as consisting of "active deposits that accrete both laterally and vertically across the channel from migrating cut banks." Convex-bank floodplains form when bedload material is deposited on the inside of the bend due to helical flow. Coarse material (coarse sand and gravel) is deposited upstream at the bar head, and fine-grained suspended sediment (sand and silt) is deposited downstream due to secondary flow circulation cells (Brierley and Fryirs, 2005). Hummocks are deposits that form behind vegetation on the platform during high flow events (Figure 2.2).

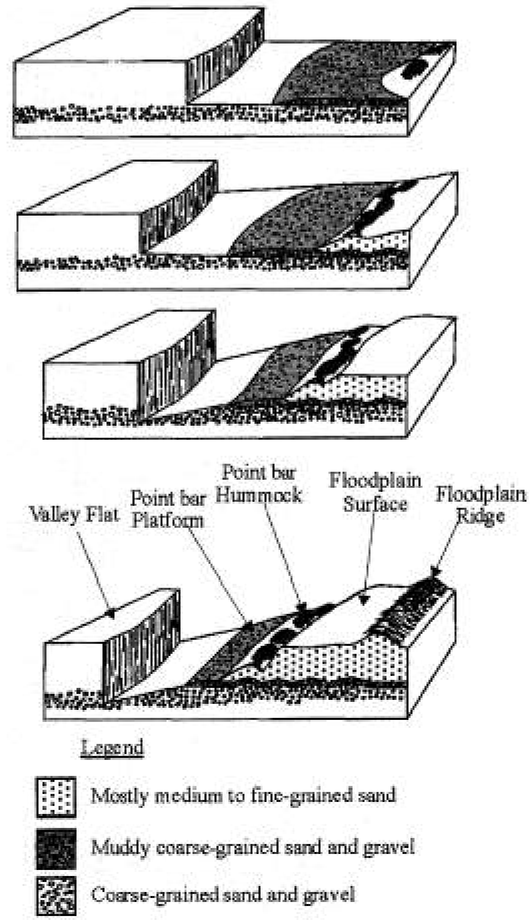

Figure 2.2: Block diagram showing the evolution of convex-bank floodplains. (Allmendinger, 2004)

Allmendinger (2004) took sediment cores along the White Clay Creek to determine how convex-bank floodplains develop in alluvial channels. Cores were taken on the same point bar monitored in this study, as well as on two point bars downstream of the study site. Allmendinger (2004) found that the point bar platform deposits consist of a bottom layer of coarse sand and gravel with a thickness of 27 cm. Above the coarse sand and gravel there is a layer of mud with an average thickness of

24 cm. In addition, multiple hummocks were present on the point bar platform that consisted of fine to medium sand with an average thickness of 30 cm. Allmendinger (2004) credits the formation of the fine to medium sand hummock deposits to grassy vegetation. Furthermore, cores taken on the upper floodplain surface showed point bar deposits below the overbank deposits. This stratigraphy signifies that convex-bank floodplains in this region evolve from lateral point bar accretion to overbank vertical accretion.

Moody and Meade (2014) documented three decades of point bar evolution along the Powder River in Montana. They used annual cross-sectional surveys to determine the magnitude of sediment eroded from age-based stratigraphic units. They found that annual net deposition was 9.0, 11.6, and 10.8 cm/yr and net erosion was 1.5, 5.3, and 7.0 cm/yr for the 3 point bars. Their results showed the development of scroll bars and chute channels and that erosion plays a significant role in the evolution of a point bar.

2.2 Evolution of Piedmont Streams

Mid-Atlantic piedmont stream morphology has been altered by agriculture, deforestation, milldam construction, urbanization, and suburbanization (Wolman and Leopold, 1957; Wolman, 1967; Jacobson and Coleman, 1986; Pizzuto et al., 2000; Walter and Merritts, 2008). The geomorphic models presented by Jacobson and

Coleman (1986) and Walter and Merritts (2008) describe the evolution of alluvial deposits in the mid-Atlantic.

Jacobson and Coleman (1986) describe the evolution of Maryland piedmont floodplains since before European settlement. They describe three periods, pre-settlement, agricultural, and very recent, which are characterized by different fluvial conditions (Figure 2.3). The pre-settlement period prior to 1730 was characterized as having thin laterally accreted sand and gravel deposits below thin fine-grained overbank deposits. From 1730 to 1930, agricultural practices caused a large increase in sediment supply and an increase in discharge. Deposits during this period consisted of thick fine-grained overbank deposits and thin laterally accreted sand deposits. Around 1930, the agricultural period ended and the sediment supply to Piedmont streams decreased. This decrease in sediment supply resulted in silt and fine-grained sand to be removed from storage and coarse sand and gravel to form lateral accretion deposits such as point bars (Jacobson and Coleman, 1986).

Walter and Merritts (2008) describe most mid-Atlantic floodplains as being fill terraces formed as a result of milldams and increased agriculture (Figure 2.4). Beginning in the 17th century and ending in the early 20th century, milldams were built throughout the eastern United States. These dams trapped fine sediment and built up the floodplain. The resulting sediments that filled in millponds are described as being thick and fine-grained, similar to those described by Jacobson and Coleman (1986). Walter and Merritt's (2008) model explains that modern channel-bed sediment consists of sand and gravel rather than the fine material that was deposited due to milldam construction. Once a dam breaches, the channel incises into the fine-grained sediment and the shear stress increases. This increase in shear stress allows coarse material to be transported downstream (Walter and Merritts, 2008).

The models described by Jacobson and Coleman (1986) and Walter and Merritts (2008) both show that during the agricultural period, there was an increase in sediment supply leading to thick, fine-grained floodplain deposits. Since 1930, agriculture has decreased and abandoned milldams have failed, leading to a change in floodplain formation. Recent floodplain formation consists of slow lateral accretion of coarse-grained material (Allmendinger, 2005; Pizzuto and Meckelnburg, 1989) and slow vertical accretion of fine-grained material (Allmendinger, 2007; Bain and Brush, 2005).

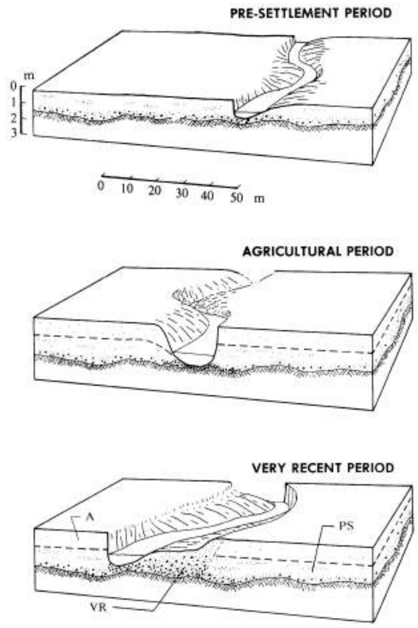

Figure 2.3: Floodplain development in the Maryland Piedmont (Jacobson and Coleman, 1986).

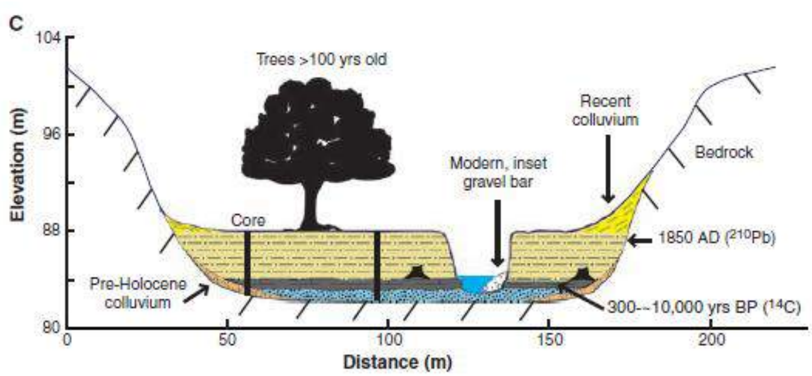

Figure 2.4: Conceptual model representing typical mid-Atlantic stream stratigraphy. Thick overbank deposits due to milldam construction and modern gravel bars are illustrated (Walter and Merritts, 2008).

2.3 Terrestrial Laser Scanning

TLS is a high-resolution remote sensing technique that uses LiDAR to scan a three-dimensional surface. TLS are able to survey three-dimensional surfaces with better coverage of the topography than traditional survey techniques. Scans produce precise and accurate 3D measurements of topographic features that can be made into DEMs and compared to repeat surveys to analyze morphological changes.

Recently, TLS has been used to observe small scale changes to features associated with rivers (O’Neal and Pizzuto, 2010; Kasvi et al., 2013; Picco et al., 2013; Starek et al., 2013; Kuo et al., 2014). O’Neal and Pizzuto (2010) used TLS to determine bank erosion rates by comparing repeat scans along the South River in Virginia. Similarly, Starek et al. (2013) used TLS to measure bank erosion of legacy sediment in a Piedmont stream located in Raleigh, North Carolina. Picco et al. (2013) observed erosion and deposition after flooding events of a gravel-bed braided river using TLS.

The use of TLS to monitor a point bar will greatly improve our knowledge on how point bars evolve. Kasvi et al. (2013) used TLS to observe the effects of a flood on two point bars along the Pulmanki River in northern Finland. They found that differing discharges modified the point bar morphology. Additionally, they found that the shape of the point bar itself affected the flow of the river. On the two point bars measured, 56% and 44.5% of the point bar area experienced net erosion due to the flood event (Kasvi et al., 2013).

2.3.1 TLS Challenges

Although TLS has proven to be an effective tool for use in the field of geomorphology, there are challenges that arise with data acquisition and processing. TLS usually requires multiple setup locations to get the coverage necessary at a specific study site. In addition, individual scan locations need to be stitched together, which increases the post-processing time and introduces error into the resulting model. Some locations may be remote or have terrain that makes it difficult or impossible to reach with all the equipment that is necessary for scanning. Furthermore, point clouds can have tens to hundreds of millions of points, which can be difficult to work with depending on the software used to process the data.

Uncertainty error is an issue when dealing with elevation models created from survey data. With TLS, errors arise from various sources such as the internal instrument error, individual scene registration, repeat scan referencing, surface roughness, surface interpolation, etc. To separate noise from true geomorphic change in a DoD analysis, an estimate of the uncertainty needs to be quantified from instrument, positional, and roughness error.

In geomorphology, it is common practice to use a spatially uniform error analysis, which applies the same error to every cell of a DEM. Previous studies have quantified this error by using the factory reported instrument error, assessing the co-registration and scan to scan referencing errors (O’Neal and Pizzuto, 2010; Kane, 2015), and by looking at the variance between fixed ground control points recorded by different survey methods. The uniform error for each DEM is propagated into the DoD and a minimum Level of Detection ($_{min}$LoD) threshold is applied to remove anything that could be considered noise. This technique discards true geomorphic change in areas that have uncertainties lower than the $_{min}$LoD (areas with low slope, low roughness, and high point density) and does not discard enough information in areas with uncertainty greater than the $_{min}$LoD.

Wheaton (2010) developed a Fuzzy Inference System to account for spatially variable errors within DEMs. This technique takes into account point density, roughness, slope, etc., and estimates an error value for every cell within a DEM. The error is then propagated into the DoD on a cell by cell basis and probabilistic thresholding can be used to remove values below a given confidence interval. The advantage of a spatially variable analysis, over a uniform error analysis, is that areas that were previously thresholded out, can now be included in the calculations. Additionally, cells that may have vegetation, or values that are not representative of the surface, can be removed individually. Recently, this technique has been used extensively in the field of fluvial geomorphology (Wheaton, 2010; Kasvi et al., 2013; Kuo et al., 2014).

Chapter 3

STUDY AREA

This study focused on one point bar located 5.3 km north of Newark, Delaware along the White Clay Creek (Figure 3.1). The White Clay Creek drains into the Christina River, which is a tributary of the Delaware River. There are three main branches that join to form White Clay Creek before the Delaware border: West Branch, Middle Branch and East Branch. The point bar is located approximately 1.35 km downstream from where the main stem of the White Clay Creek crosses the Pennsylvania-Delaware border (Figure 3.1).

The point bar is approximately 100 meters long and 15 meters wide at its widest point. Sediment on the point bar ranges in size from mud to cobbles. The upstream end of the point bar is relatively flat and transitions into more of a sloping surface as you move further downstream towards the apex of the meander bend. At this point, there is a well-developed scroll bar and chute channel. The downstream end of the bar consists mainly of sand, and has a steep slope connecting the channel bottom to the upper floodplain surface. During the winter and early spring, there is little vegetation on the bar. Small clusters and rows of grass are present on the scroll bar and scattered throughout the chute channel. Small saplings have started to grow at two locations on the scroll bar. Much of the vegetation was stripped from the surface during the April 30, 2014 flood. Figure A.1 shows photos of each scan surface.

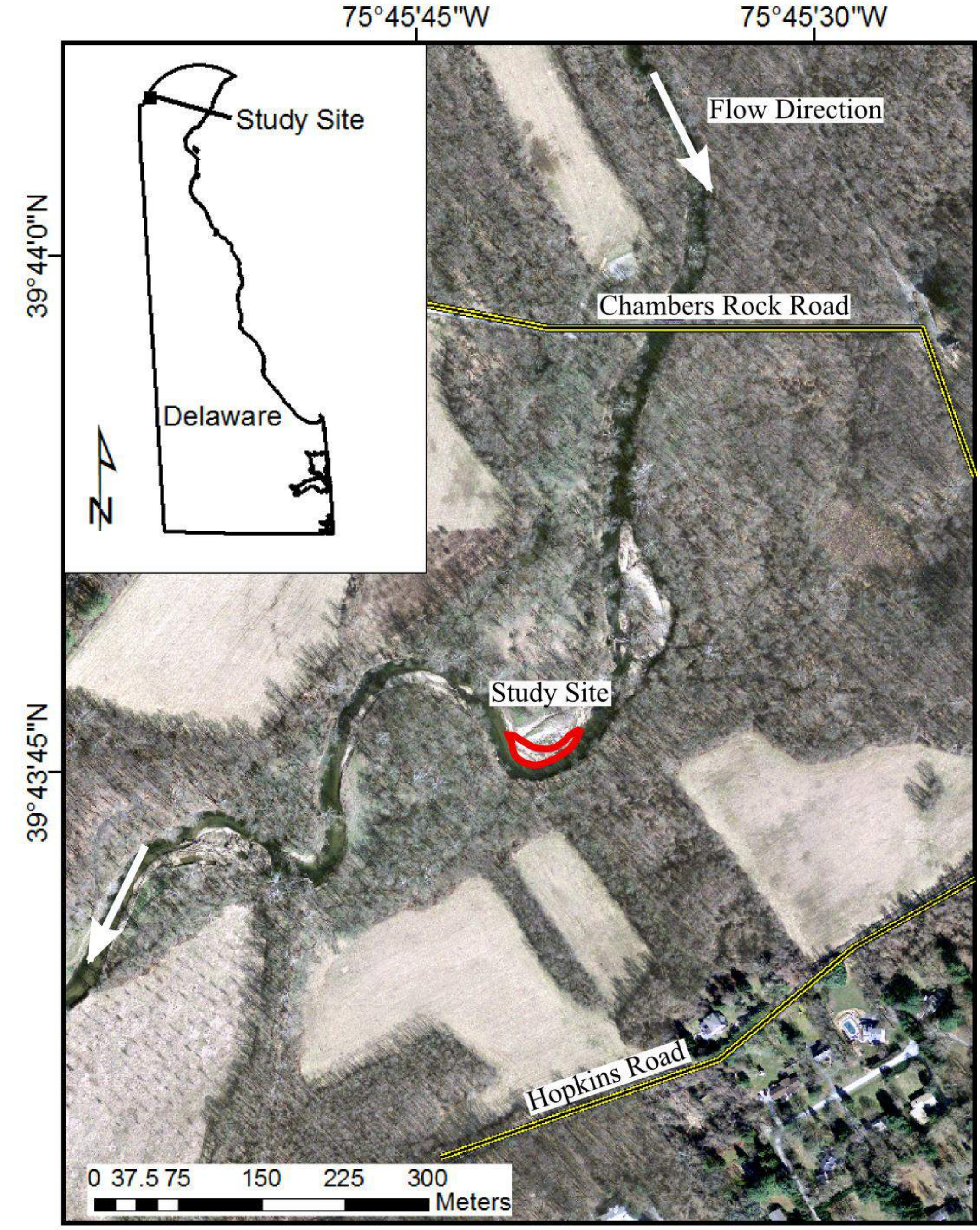

Figure 3.1: Site map showing the location of the study site along the White Clay Creek near Newark, Delaware. The scanned area is outline in red and flow direction is from north to south.

The bedrock of the White Clay Creek Watershed is dominated by pelitic schist and gneiss, with layers of fine to medium-grained amphibolite from the Wissahickon Formation (Ordovician) (Schenck et al., 2000). The study site is in an alluvial reach of the river that is underlain by the Wissahickon Formation. About 2.0 km upstream from the study site, the White Clay Creek flows through a section of the Cockeysville Marble (Cambrian) and the Baltimore Gneiss (Precambrian) (Schenck et al., 2000).

The White Clay Creek can generally be classified as a single channel alluvial river, with frequent pools and riffles. Bed material ranges in size from sand and mud to cobbles. Many of the bends have developed point bars and steep cut banks composed of fluvial deposits. Occasionally, there are reaches dominated either by bedrock underlying the channel or along its banks. The river is located in a humid subtropical/humid continental region with an average temperature of 54°F. Average rainfall is 1.14 m/yr (Delaware Climate Information, 2010).

Hydrologic data were obtained from U.S. Geological Survey (USGS) stream gaging stations 01478650 at Newark, Delaware and 01478245 near Strickersville, Pennsylvania. The Newark, DE and the Strickersville, PA stations have 22 and 19 years of continuous data, respectively. These two stations were chosen because they are the closest stream gages upstream and downstream of the study site (Figure 3.2).

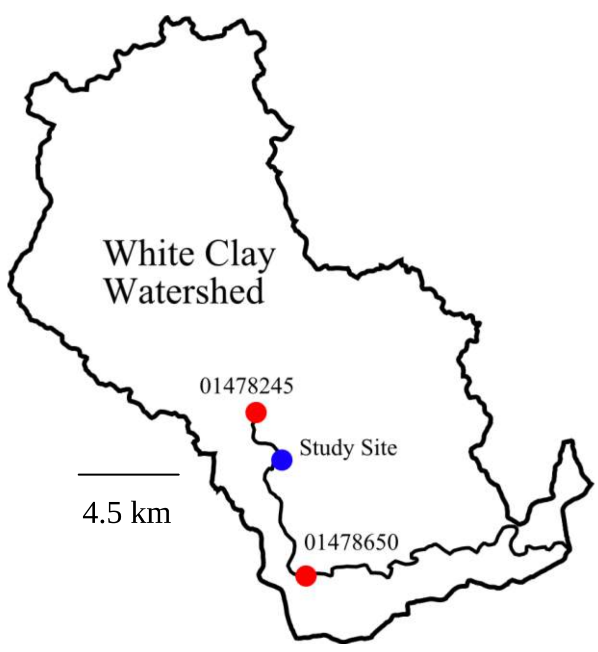

Figure 3.2: Location of the study site (blue circle) and the two closest stream gages (red circles) in the White Clay Watershed.

Chapter 4

METHODS

4.1 Terrestrial Laser Scanning

Scans of the point bar were completed on April 11, 2014 (Scan 1), May 8, 2014 (Scan 2), and April 16, 2015 (Scan 3) using a Trimble GX Advanced Terrestrial Laser Scanner. The scanner is set up on a tri-pod and rotates around a vertical axis to scan features within a user specified survey domain. The instrument calculates the distance to features by recording the return time of travel for emitted pulses of green light (532 nm) with a factory-tested vertical accuracy of approximately 1.3 mm at a distance of 100 m. At each set up location, the scanner records the azimuth, zenith, and distance measurement of the first surface reflection. The resulting three-dimensional coordinates are then placed into a local Cartesian coordinate system originating at the instrument.

The coverage and resolution of the TLS data depends on the user specified point spacing of the laser. The instrument records a greater number of laser pulse returns from features that are closer than those that are farther away. For this study, 2.5 cm incremental steps at distances of 50 m and 100 m, depending on the location and the day of the scan, were used. This allowed us to get the appropriate coverage needed since most scan distances were less than 50 m.

4.1.1 TLS Field Work and Data Collecting

At the study site, four benchmarks were installed by pouring concrete into 0.50 m deep x 0.30 m wide holes. Four milled aluminum placards were inserted into the concrete (Figure 4.1a). Each placard was numbered and labeled, and allowed for spheres to be set up on the benchmarks in the same location before every scan. Seven reflective targets (0.08 m ceramic spheres) were set up at visible locations throughout the study site, including one at each benchmark (Figure 4.1b). Spheres were left untouched after setup and were numbered within the TLS software so that the individual scenes could be matched based on the modeled central points of the spheres.

a.)  b.) 

Figure 4.1: a.) Concrete benchmark with aluminum placard installed. b.) Spherical reflective targets that were set up over benchmarks and visible scanning locations throughout the study site.

At each scanner setup location, we performed a separate, focused, high-resolution scan directed at each visible sphere. This ensured accurate co-registration of the scans in post-processing. For every scanned point, the instrument recorded the local XYZ coordinates, the return intensity, and the true-color RGB. For the first two scans, seven setup locations (scenes) were needed to cover the surface of the point bar. Two scenes were shot from the opposite bank and five along the chute channel of the point bar. For the third scan, six setup locations were needed to cover the surface of the point bar. We scanned on both sides of topographic features to reduce shadow effects.

4.1.2 TLS Data Processing

4.1.2.1 Registration

Post-processing of the point clouds required the seven individual scenes to be registered to each other based on the XYZ locations of the sphere's modeled central point. Every sphere within an individual scene was aligned to its matching sphere from a different scene, using Trimble's RealWorks Survey 5.0.3. This resulted in a final co-registered point cloud with all of the individual scenes stitched together based on the location of common sphere's (Figure A.2). A root mean square error (RMSE) of the distance between the matched spheres coordinate pairs was calculated to assess error in fit. This error represented the difference between a predicted location and the observed location for each sphere. We used the maximum RMSE value calculated for each day's scan and refer to it as the registration error. This error can arise from accidental sphere movement, movements of the TLS station, or from matching spheres scanned at farther distances.

4.1.2.2 Georeferencing

Upon completion of the registration process, each scan was in its own arbitrary coordinate system. In order to align the three scans, the first scan was georeferenced to Delaware State Plane NAD1983 FIPS 0700 so that the resulting DEMs could be projected in ArcGIS. The latitudinal and longitudinal coordinates of each benchmark were determined in the field using a Trimble GPS. The coordinates were converted to

State Plane NAD 1983 (Table 4.1) and a point file was created. The benchmark coordinates of the scan 1 point cloud were aligned to the benchmark coordinates of the GPS using CloudCompare (CloudCompare 2.5, 2014). This resulted in a high positional error (RMSE ≈ 1.0 m), due to the error associated with the GPS unit. For the purpose of this study, we were not concerned with this georeferencing error and all subsequent scans were aligned based on the registration of known points identified in each survey.

Benchmark	X (m)	Y (m)	Z (m)
1	170452.609	192040.944	35.00
2	170491.994	192052.321	35.38
3	170434.272	192013.177	35.55
4	170528.054	192061.110	35.88

Table 4.1: Coordinates of benchmarks referenced to Delaware State Plane NAD1983 FIPS 0700.

After georeferencing the first scan, scan 2 was aligned to scan 1 and scan 3 was aligned to scan 2. This allowed all scans to be georeferenced, while maintaining a high level of positional accuracy between subsequent scans. The alignment process is similar to the registration process, but aligns permanent markers, such as benchmarks or logs, from repeat scans rather than spheres from individual scenes. This step can be tedious, as it is important to pick points that are in the same location to minimize the alignment error. Once the scans were aligned, a visual inspection was completed to ensure the geometry of the point clouds were correct. As with the registration error, the referencing process output RMSE values for points used in aligning the scenes. The maximum RMSE value for each repeat scan was recorded and we refer to this as the referencing error. It is important that this error is minimized, so that repeat scans are aligned as accurately as possible. When differencing the two models, errors in alignment would result in inaccurate erosion and deposition calculations. Once the referencing process was complete, the point cloud was edited to remove unnecessary points outside the area of interest.

4.1.2.3 Vegetation Removal

Vegetation was removed from each scan so that only bare earth or low vegetation points remained. There was little vegetation in the study area, but some small saplings, bushes, and grasses were present. Vegetation was removed using the CANUPO classifier plug-in (Brodu and Lague, 2012) for CloudCompare (CloudCompare 2.5, 2014). This method uses a multi-scale dimensionality analysis that characterizes features, such as ground, vegetation, water, and gravel, according to their geometry. At each location in the point cloud, the geometry of the points is analyzed at different scales to determine if it is 1D, 2D, or 3D.

To run the plug-in, classifiers need to either be created from your own point cloud, or downloaded from previous users. For this study, obvious vegetation points were clipped from the point cloud and used to train the classifier. The plug-in compared the geometry of all the points in the unedited co-registered point cloud to the points used in the vegetation classifier. Points were grouped into ground and vegetation (Figure 4.2). Vegetation points missed by the CANUPO classifier were removed manually by visual inspection. The final point clouds used in creating DEMs were saved as text files and contained only bare earth or low vegetation points indistinguishable from the bare earth points.

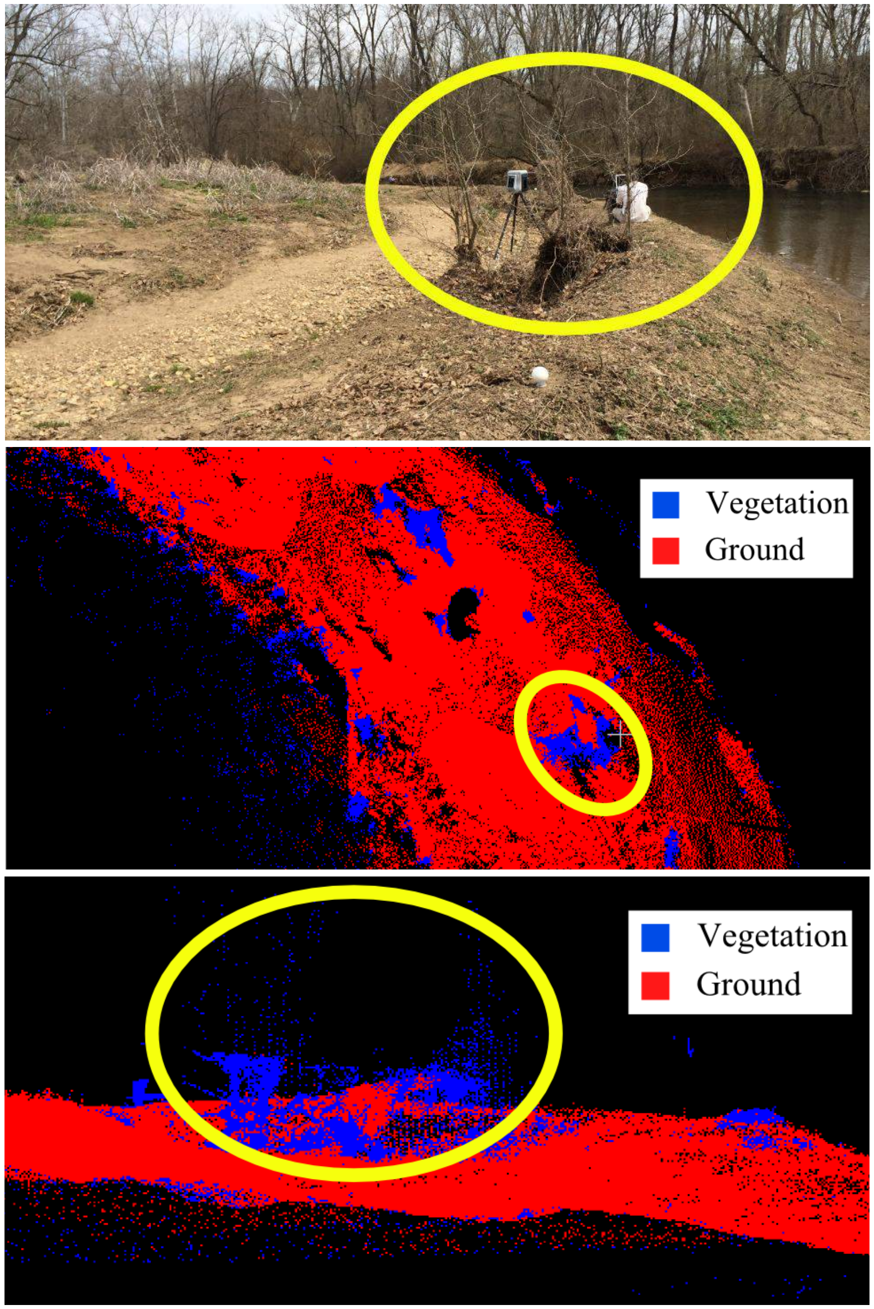

Figure 4.2: a.) Photo showing vegetation growing on the scroll bar. b.) Plan view of the point cloud with vegetation classified as blue and ground classified as red. c.) Cross sectional view of the classified point cloud. The yellow circle indicates the same cluster of vegetation.

4.2 Digital Elevation Model Generation

The edited ASCII files were opened in ArcMap (ESRI ArcMap 10.2, 2014) by adding the XYZ coordinates. In order to create accurate DEMs, the ground surface was interpolated using the XYZ points. This was done using the Create TIN tool. A TIN (Triangular Irregular Network) is a vector-based representation of the terrain surface. The procedure uses XYZ points as nodes and connects them with contiguous triangles through Delaunay triangulation. Once the TIN model was created, it was edited to remove nodes that interpolated areas of no data. For example, nodes along the water's edge and nodes within the concave part of the scan that were connected to areas outside the area of interest were removed. In addition, gaps in the point cloud where vegetation was removed were connected and needed to be removed.

DEMs were created from the TIN models using the TIN to Raster tool. When creating DEMs that will be compared to one another, it is important that they share the same processing extent and cell size. We used a cell size of 0.1 m x 0.1 m for all 3 DEMs. The extent was determined by examining the left, right, top, and bottom coordinates of each TIN model. The maximum left and bottom coordinates were rounded down to the nearest integer. The maximum right and top coordinates were rounded up to the nearest integer. These coordinates were used in creating all of the DEMs to ensure that the extents and cell size matched. DEMs were created using natural neighbor interpolation of the TIN nodes. At each query point, a weight is applied to the closest subset of samples and an elevation value is assigned that falls within the range of the samples. Since vegetation was previously removed from the point clouds, it was assumed that the DEM was a good representation of the bare earth surface. The influence of remaining vegetation points on terrain representation accuracy is minimized in the natural neighbor interpolation because vegetation elevations are considered outliers and assigned less weight.

Scan 2 had a larger coverage area because deposition extended the point bar in the downstream direction. In order to account for some of this deposition, an interpolated surface was created for the area missed by scan 1 by connecting the cells at the water's edge in the first two DEMs. The water's edge of scan 2 is likely to have been at a higher elevation than the pre-flood channel bottom at that location. This signifies that our estimate of the deposition that occurred where the point bar was extended is conservative. For each DEM, the water's edge cells were clipped. The clipped DEM cells from each model were then combined using the Cell Statistics tool. The combined DEM was converted to points and the surface between the points was interpolated using a TIN. Once the TIN was edited, it was converted to a DEM and was added to the original scan 1 DEM using the Cell Statistics tool.

DEMs were loaded into the Geomorphic Change Detection (6.1.3) plug-in in order to difference the two surfaces. Since a DEM represents sets of equally spaced points, they can easily be differenced if they are aligned properly. A thresholded DoD was created for each subsequent scan by subtracting the older scan from the newer scan and removing errors that fall between the ${}_{min}$LoD values. Figure 4.3 outlines the data processing steps involved with our TLS data.

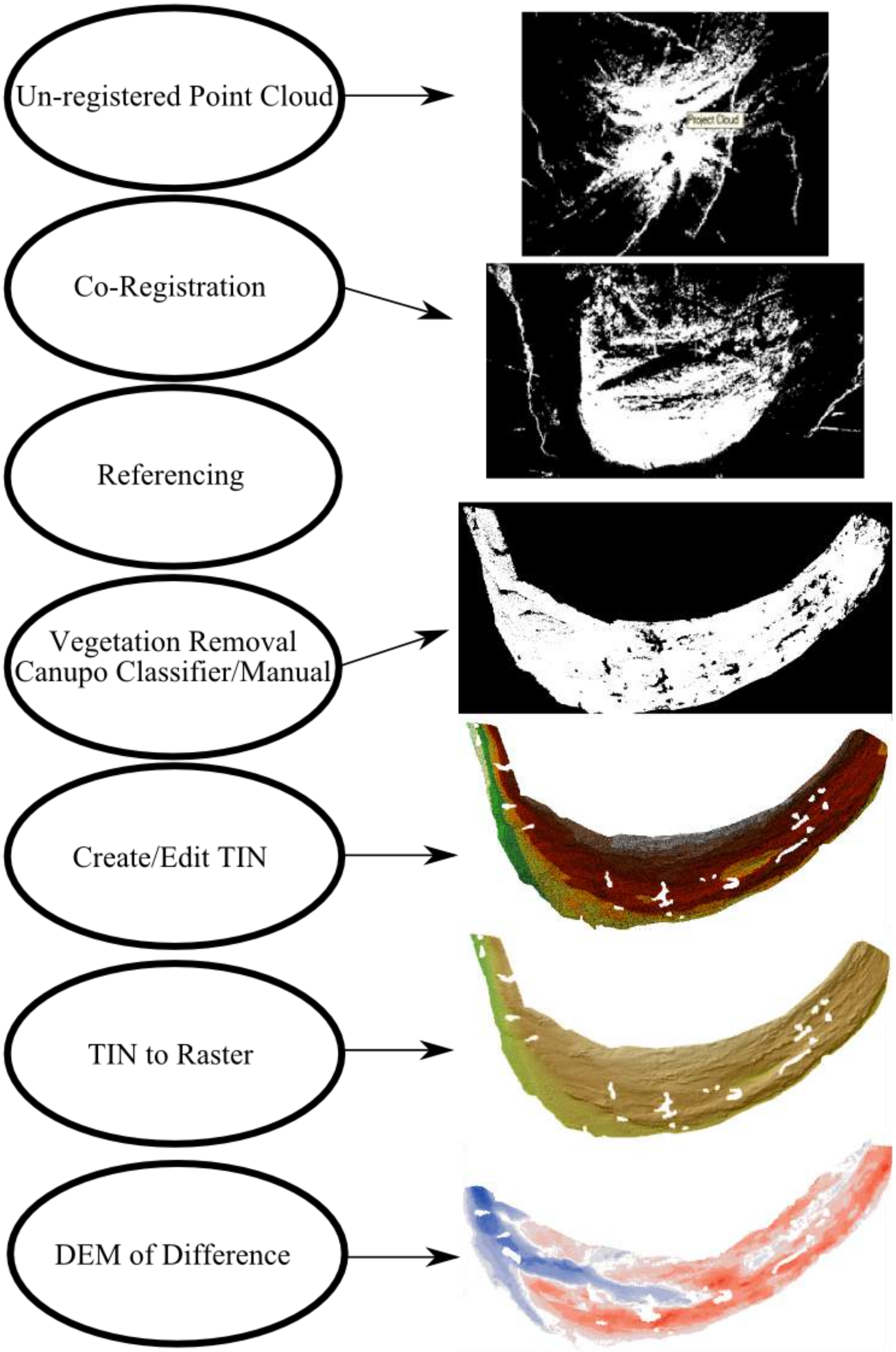

Figure 4.3: Flow chart of the methods used to produce final DoDs.

4.3 Error Analysis

To assess the uncertainty in our data and determine the $_{min}$LoD, multiple error sources were analyzed. First, we looked at positional uncertainty that arises from instrument error, registration and referencing. This is uncertainty that would affect the location of points within the point cloud. To account for this error, a summation of the factory reported instrument error and the maximum RMSE values of the registration and referencing process was calculated.

Roughness of the point bar surface was also analyzed to determine the range of elevation values that may fall within an individual DEM pixel. This uncertainty represents vertical variations and is a result of interpolating point cloud data into a gridded surface. Three 1.0 m x 1.0 m areas of the May 8, 2014 point cloud were clipped and analyzed. These areas represent the typical grain size (sand and gravel) of the point bar. A minimum value DEM and a maximum value DEM with 0.1 m x 0.1 m grid spacing was created of each clipped area. The minimum value was subtracted from the maximum value and the RMSE was determined and used as a proxy for surface roughness.

4.4 Cross Sections

Cross sections were created to show the magnitude of erosion and deposition along the point bar after each high flow event. Five transects were chosen starting from the upstream end of the point bar and ending at the downstream end. Elevation data from each DEM was exported from GIS and elevation profiles were plotted. Subsequent scan profiles were plotted on the same chart so that elevation comparisons could be made.

4.5 Flow Frequency Analysis

Data from both the Newark, DE and Strickersville, PA stream gages were used to determine the return period of the flood event that occurred on April 30, 2014, between scan 1 and scan 2, using a Log-Pearson Type III analysis and annual peak discharge (Bulletin 17B, 1981). Return period, otherwise known as recurrence interval, is the time which events of a given magnitude are expected to be equaled or exceeded. For example, a 20 year flood has a likelihood of being equaled or exceeded once every twenty years, or a 5% chance of being equaled or exceeded in a given year.

For each station, the annual peak discharge was determined and ranked from largest to smallest. The variance and standard deviation were calculated by:

$$var(x) = \frac{\sum_i^n (x-\bar{x})^2}{n-1} \tag{1}$$

$$S = \sqrt{\frac{\sum_i^n (x-\bar{x})^2}{n-1}} \tag{2}$$

Where:

$var(x)$ = Variance of logarithms of peak discharge

S = Standard deviation of logarithms of peak discharge

x = Log of peak discharge

$\bar{x}$ = Average log of peak discharge

n = Number of events on record

A generalized regional skew (Appendix A.3) of 0.55 was used instead of the skew for each station, due to each station having less than 25 years of data. The skew coefficient was used to determine the k frequency factor values of the 2, 5, 10, 25, 50, and 100 year return periods. The predicted discharge of each return period was calculated by (Bulletin 17B, 1981):

$$Log(Q_{tr}) = \bar{x} + kS \tag{3}$$

Where:

Q_{tr} = Predicted discharge for each return period (m^3/s)

S = Standard deviation of logarithms of peak discharge

$\bar{x}$ = Average log of peak discharge

k = Frequency factor determined from regional skew coefficient

A frequency distribution was created that predicts the return period of a known flood discharge at each stream gage. Annual peak discharge values were plotted with their calculated Weibull return period (Equation 4). The Weibull equation calculates a return period for each peak discharge value, which allows for the values to easily be compared to the frequency distribution.

$$R = \frac{n+1}{m} \tag{4}$$

Where:

R = Weibull return period

n = Number of events on record

m = Rank of each event

4.6 Grain Size Analysis

On June 6, 2014, a survey of the point bar was completed in order to create a surface grain size map of the study site after the April 30, 2014 flood. It is important to note that this map only represents one snapshot in time and it cannot be used to predict the grain size of previous or subsequent point bar surfaces. Unfortunately, due to the timing of the storm event, a grain size map of the pre flood surface was not completed.

A TOPCON total station was set up over benchmark 1. Eight cross sections consisting of a total of 58 locations on the point bar surface were surveyed using a rod and a reflective target that allowed the grain size map to be aligned with the second scans DEM (Figure A.4)

At each survey point, surface grain size was determined by observing hand samples. Sediment was grouped into the following categories based on the Wentworth grain size classification: muddy sand, sand, sand and gravel, and gravel. Gravel at the study site ranged in size from granules to cobbles (>2.00 mm - <256 mm). Benchmark locations were used to align survey points of the second scans DEM. A final grain size map was interpolated from the point data and the DEM of the second scan.

Chapter 5

RESULTS

5.1 Flow Frequency Analysis

The Log Pearson Type III analysis for both the Newark, DE and the Strickersville, PA stream gages indicated that the flood event on April 30, 2014 was equivalent to the 6.1 year flood. Since both analyses indicated the same return period, only the results of the Newark, DE stream gage are presented here. Daily discharge values for the entire study period are presented in Figure 5.1. The discharge values that correspond to the 2, 5, 10, 25, 50, and 100 year return periods are 104.3 m^3/s, 215.3 m^3/s, 328.5 m^3/s, 535.8 m^3/s, 744.1m^3/s, and 1009.8 m^3/s (Table 5.1) (Figure 5.2). The Weibull recurrence intervals for annual peak discharge were also plotted on Figure 5.2, so that the discharge values could easily be compared to the Log Pearson Type III analysis (Table 5.2) (Figure 5.2).

Between scan 2 and scan 3, there were three small events with return periods around 1.0 – 1.25 years. The largest event during this period occurred on March 11, 2015, which had a discharge of 48.1 m^3/s (Figure 5.2). These events were not at bankfull, but did cover much of the point bar surface. After each event, there was evidence that the point bar was submerged. There were small deposits of sand as well as chunks of ice and pieces of wood that were left behind when the water level receded. There was no ice on the flat upper portion of the floodplain.

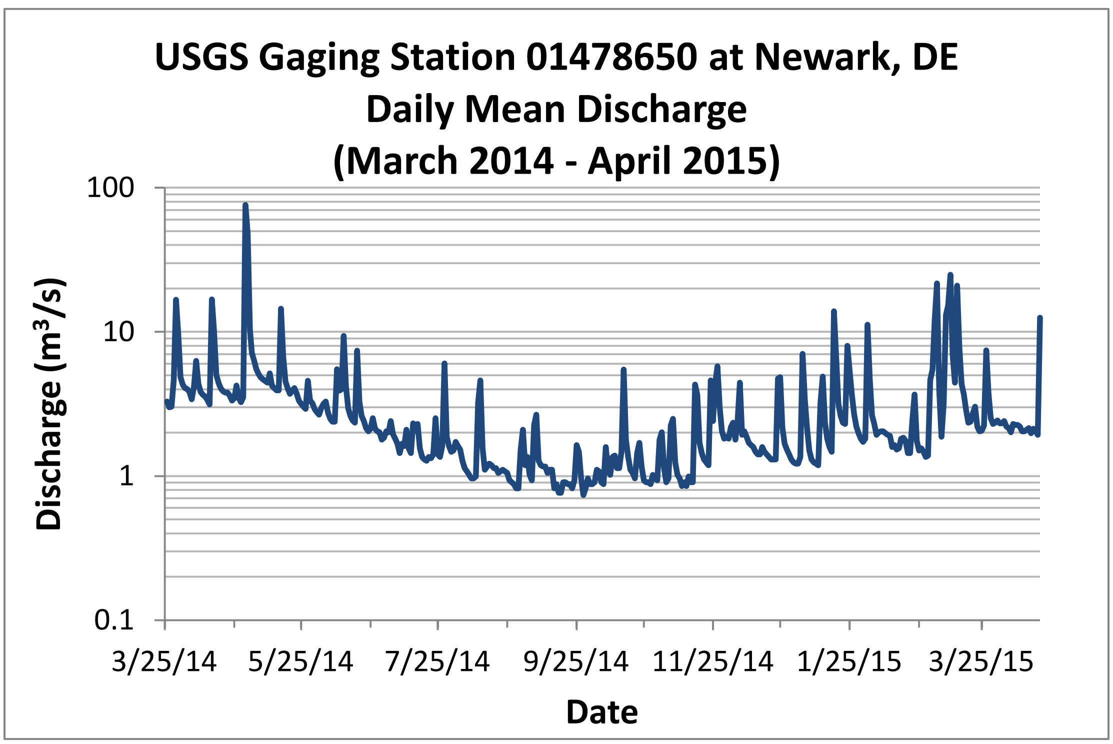

Figure 5.1: Discharge values from March 2014 through April 2015 for USGS gaging station 01478650 at Newark, Delaware.

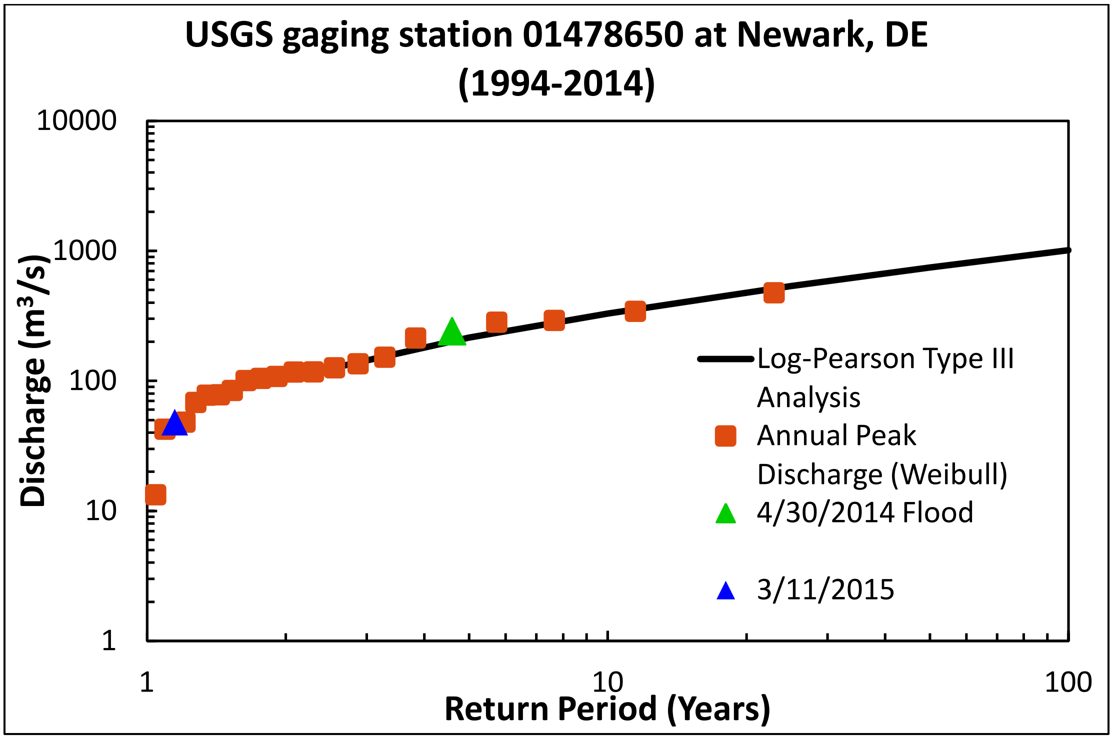

Figure 5.2: Log Pearson Type III distribution (black line) with annual peak discharge (orange squares) for USGS gaging station 01478650 at Newark, DE. The April 30, 2014 flood is shown as a green triangle and the March 11, 2015 event is shown as a blue triangle.

Return Period (Years)	k (Skew Coefficient = 0.55)	Q (m^3/s)
2	-0.091	104.3
5	0.804	215.3
10	1.3255	328.5
25	1.9295	535.8
50	2.335	744.1
100	2.712	1009.8

Table 5.1: Results of the Log Pearson Type III analysis showing return period, the corresponding frequency factor (k) values and discharge (Q).

Date	Discharge (m^3/s)	RI (Years)	Probability (yr^{-1})
9/16/1999	475.72	23.00	0.04
9/28/2004	342.63	11.50	0.09
8/28/2011	291.66	7.67	0.13
9/15/2003	282.60	5.75	0.17
4/30/2014	240.98	4.60	0.22
1/19/1996	213.51	3.83	0.26
1/28/1994	152.06	3.29	0.30
10/19/1996	135.35	2.88	0.35
12/17/2000	126.01	2.56	0.39
3/2/2007	117.23	2.30	0.43
6/3/2006	116.95	2.09	0.48
12/26/2009	108.17	1.92	0.52
6/28/2013	104.49	1.77	0.57
11/28/2004	100.52	1.64	0.61
12/12/2008	84.38	1.53	0.65
3/9/1995	78.15	1.44	0.70
3/21/2000	77.59	1.35	0.74
11/23/2011	68.24	1.28	0.78
2/13/2008	48.14	1.21	0.83
3/11/2015	48.14	1.15	0.87
1/23/1998	42.48	1.10	0.91
3/20/2002	13.31	1.05	0.96

Table 5.2: Summary of data obtained from USGS stream gage 01478650 at Newark, DE, including the calculated Weibull recurrence intervals and exceedence probabilities. The April 30, 2014 flood and the March 11, 2015 event are highlighted in yellow.

5.2 Digital Elevation Models

The scan on April 11, 2014 had a total of 1,554,330 points that were edited down to 1,085,043 points. The maximum registration error was 0.90 cm. A TIN (Figure A.5) and DEM (Figure 5.3) were created from the scan 1 points. Elevation values in the DEM ranged from 33.31 m to 35.25 m.

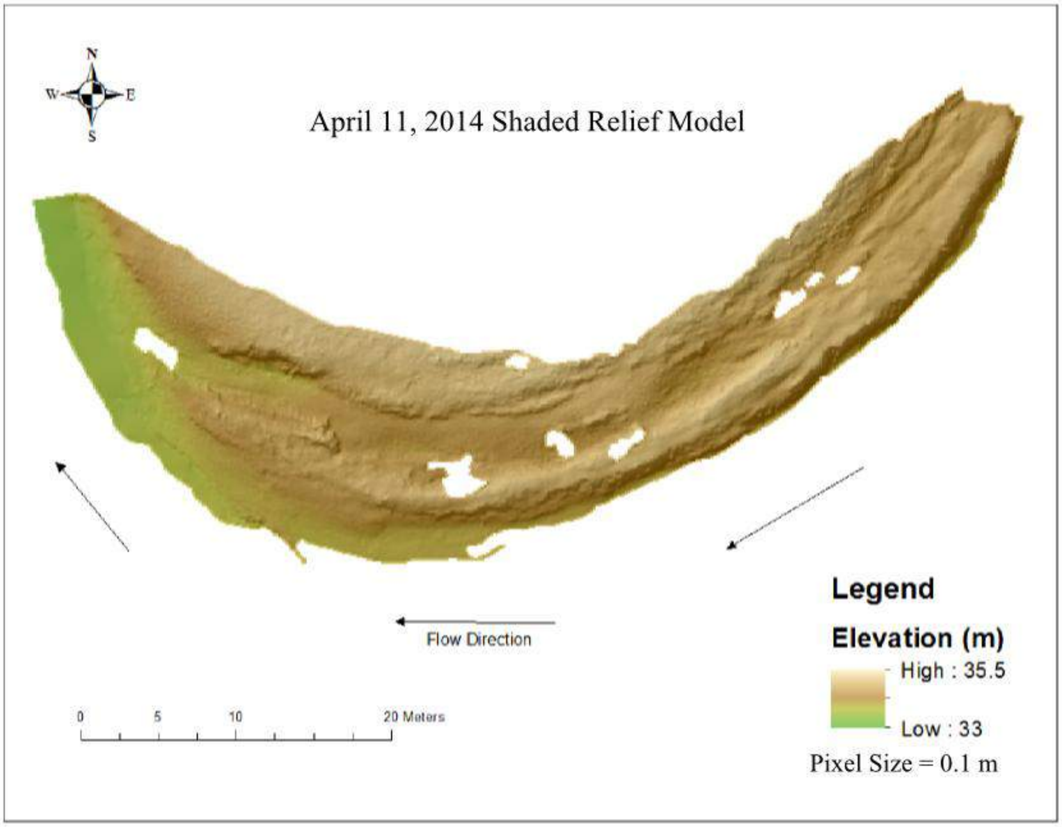

Figure 5.3: Digital Elevation Model with Hillshade of the April 11, 2014 scan. Higher elevations are shown in light brown, lower elevations are shown in green. Areas of no data within the DEM represent points that were removed due to vegetation.

The scan on May 8, 2014 had a total of 5,752,579 points that were edited down to 3,581,325 points. The maximum registration error was 0.92 cm and the referencing error was 0.72 cm. A TIN (Figure A.5) and DEM (Figure 5.4) were created from the scan 2 points. Elevation values in the DEM ranged from 33.11 m to 35.33 m.

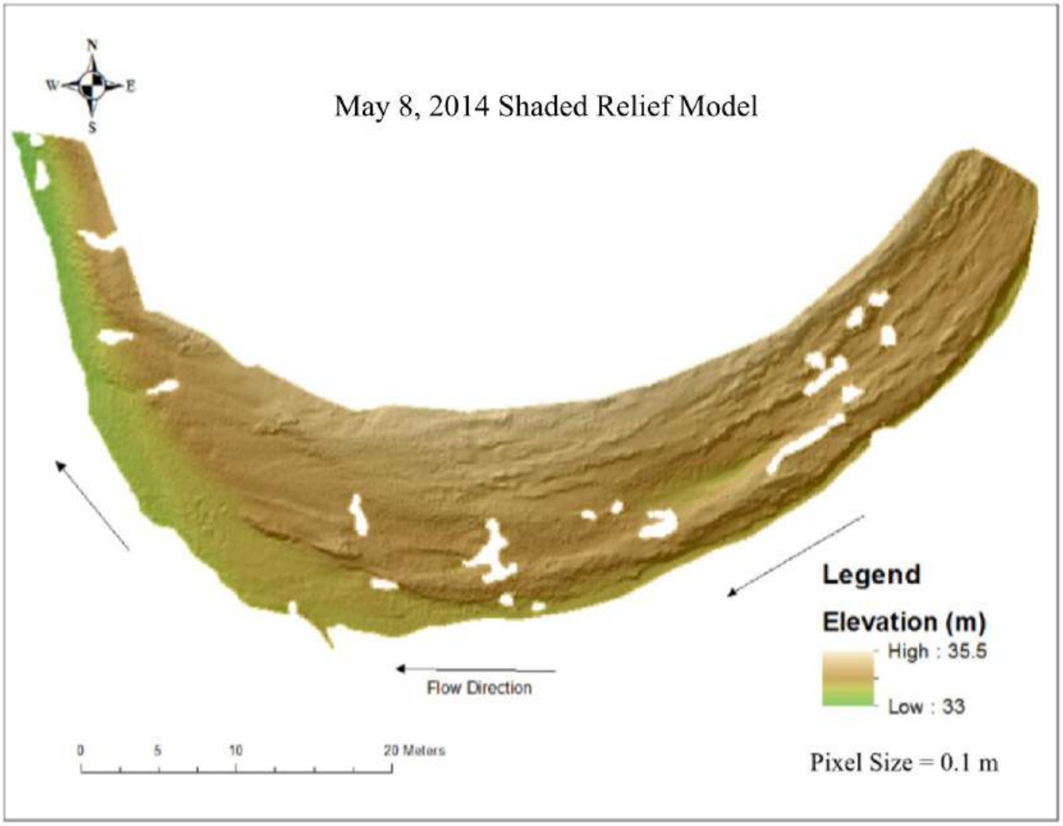

Figure 5.4: Digital Elevation Model with Hillshade of the May 8, 2014 scan. Higher elevations are shown in light brown, lower elevations are shown in green. Areas of no data within the DEM represent points that were removed due to vegetation.

The scan on April 16, 2015 had a total of 7,334,024 points that were edited down to 4,836,467 points. The maximum registration error was 0.97 cm and the referencing error was 1.00 cm. A TIN (Figure A.5) and DEM (Figure 5.5) were created from the scan 3 points. Elevation values in the DEM ranged from 33.05 m to 35.44 m.

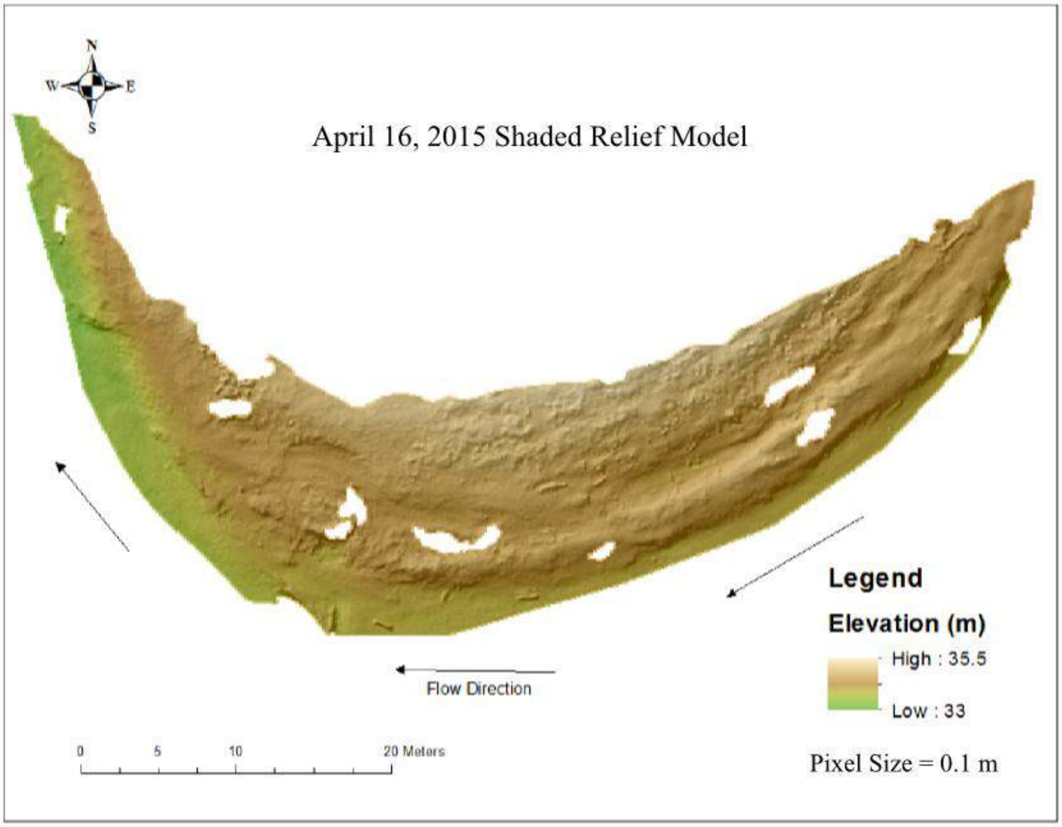

Figure 5.5: Digital Elevation Model with Hillshade of the April 16, 2015 scan. Higher elevations are shown in light brown, lower elevations are shown in green. Areas of no data within the DEM represent points that were removed due to vegetation.

5.3 Error Analysis

A summary of the positional errors for each DEM is presented in Table 5.3. The total positional error for DoD1 was 2.80 cm. The total positional error for DoD2 was 3.15 cm. These values represent maximum positional error and are conservative estimates which take into account x, y, and z uncertainties.

Roughness was calculated for three sections of the May 8, 2014 scan. The three areas had RMSE values of 2.6 cm, 3.4 cm, and 2.1 cm with an average RMSE of

2.7 cm (Table 5.4). It is important to note that while these uncertainties are low, the actual pixel values in each DEM fall somewhere between the maximum and minimum values, since we used a TIN natural neighbor interpolation. The maximum and minimum values are therefore weighted less and the pixel value is a better representative of all the points that fall within each cell.

For each DoD, we used a $_{min}$LoD threshold of 0.03 m. We chose this value because our positional errors and roughness values all fell around 0.03 m. Since we used maximum values, we believe that this is a conservative estimate of the uncertainty that is propagated into each DoD. All pixel values that had elevation differences between 0.03 m and -0.03 m were excluded and not used in the volumetric calculations.

DEM of Difference	Scan	Instrument Error (cm)	Registration Error (cm)	Referencing Error (cm)	Total Error (cm)
DoD1	Scan 1	0.13	0.90	0.72	2.80
	Scan 2	0.13	0.92		
DoD2	Scan 2	0.13	0.92	1.00	3.15
	Scan 3	0.13	0.97		

Table 5.3: Summary of the positional errors associated with each DEM and DoD.

Section	Roughness (RMSE)
Section 1	2.6 cm
Section 2	3.4 cm
Section 3	2.1 cm
Average	2.7 cm

Table 5.4: Summary of the typical roughness errors in our TLS data.

5.4 DEMs of Difference

Subtracting the April 11, 2014 scan from the May 8, 2014 scan resulted in a DEM of Difference (Figure 5.6) with a total area of detectable change of 631.72 m^2. The total area that experienced erosion was 443.77 m^2 and the total area that experienced deposition was 187.95 m^2. The net volumetric change that occurred was -49.40 m^3. Total erosion was 88.53 m^3 and total deposition was 39.12 m^3. Average depth of erosion was 0.20 m and average depth of deposition was 0.21 m (Table 5.5). Volumetric and areal histograms were created to show the distribution of the data relative to elevation changes of a given magnitude (Figure 5.7).

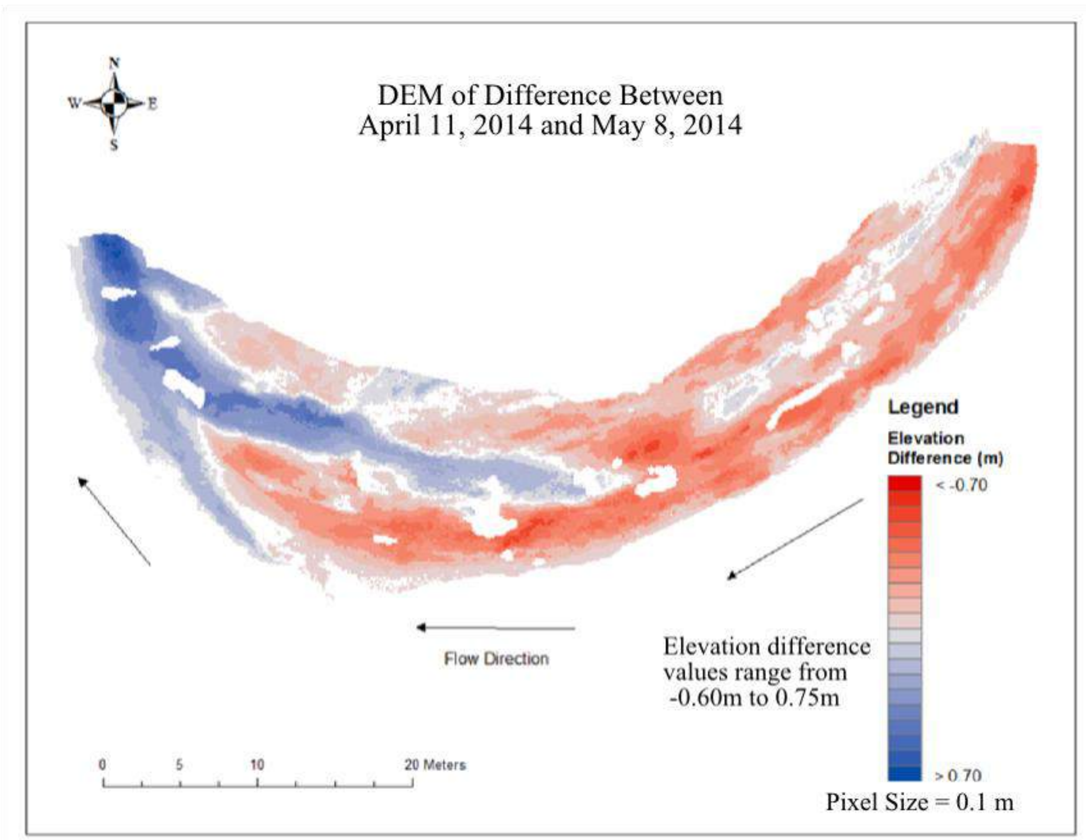

Figure 5.6: DEM of Difference between the April 11, 2014 scan and the May 8, 2014 scan. Erosion is shown in red and deposition is shown in blue. Areas of no data within the DEM represent points that were removed due to vegetation and cells that were below the $_{min}$LoD.

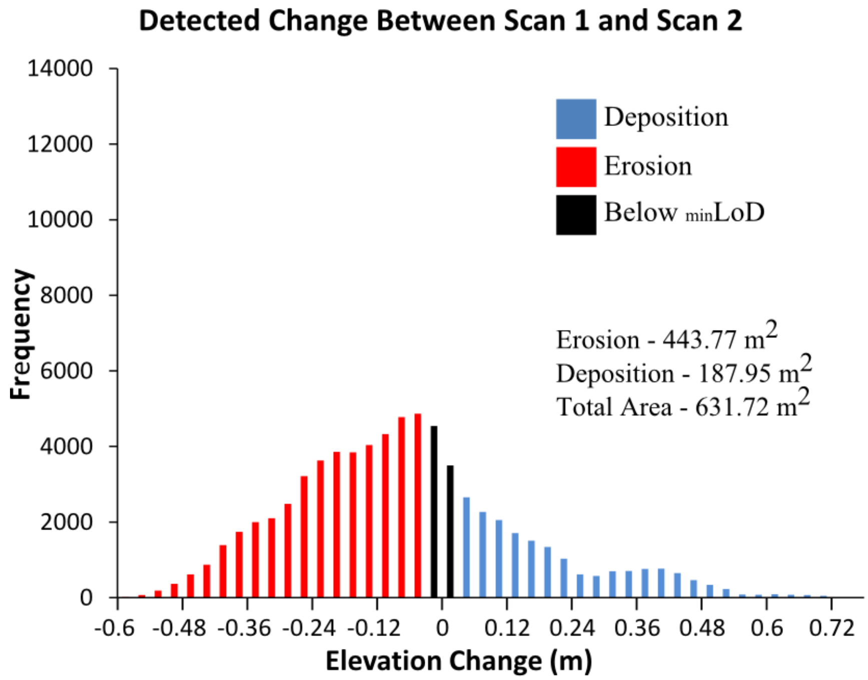

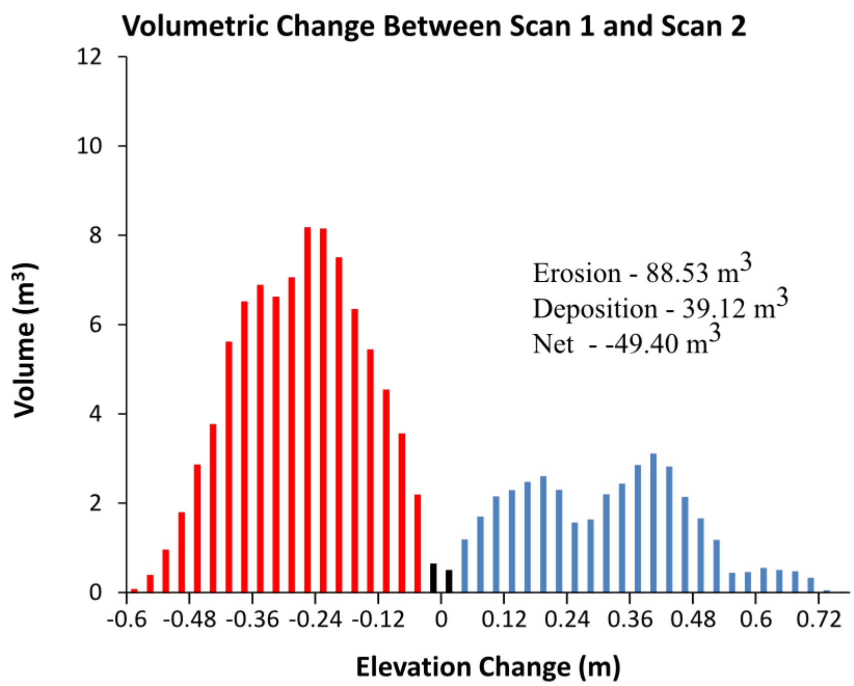

Figure 5.7: Histograms displaying cell frequency and volumetric distribution of DoD 1. Positive blue values indicate deposition and negative red values indicate erosion. Values below the 0.03 m threshold are shown in black. Written values refer to thresholded DoD.

Subtracting the May 8, 2014 scan from the April 16, 2015 scan resulted in a DEM of Difference (Figure 5.8) with a total area of detectable change of 620.74 m^2. The total area that experienced erosion was 115.10 m^2 and the total area that experienced deposition was 505.64 m^2. The net volumetric change that occurred was 40.13 m^3. Total erosion was 13.33 m^3 and total deposition was 55.46 m^3. Average depth of erosion was 0.12 m and average depth of deposition was 0.11 m (Table 5.5). Volumetric and areal histograms were created to show the distribution of the data relative to elevation changes of a given magnitude (Figure 5.9).

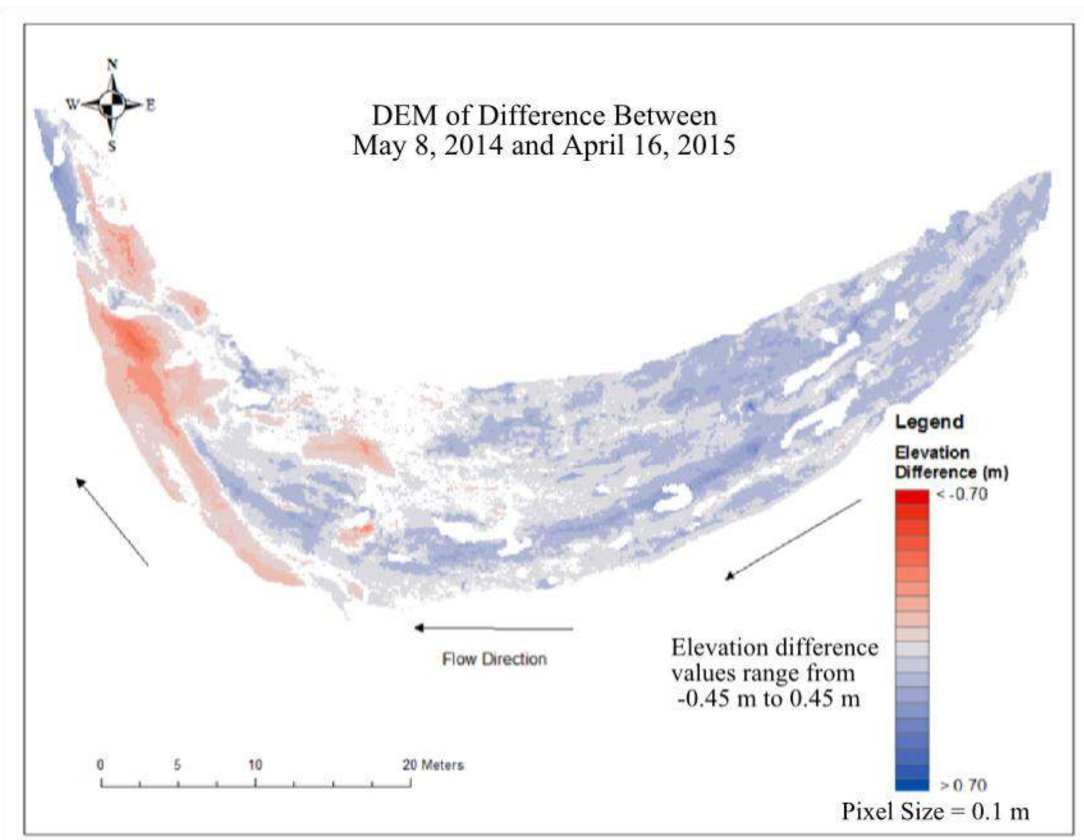

Figure 5.8: DEM of Difference between the May 8, 2014 scan and the April 17, 2015 scan. Erosion is shown in red and deposition is shown in blue. Areas of no data within the DEM represent points that were removed due to vegetation and cells that were below the $_{min}$LoD.

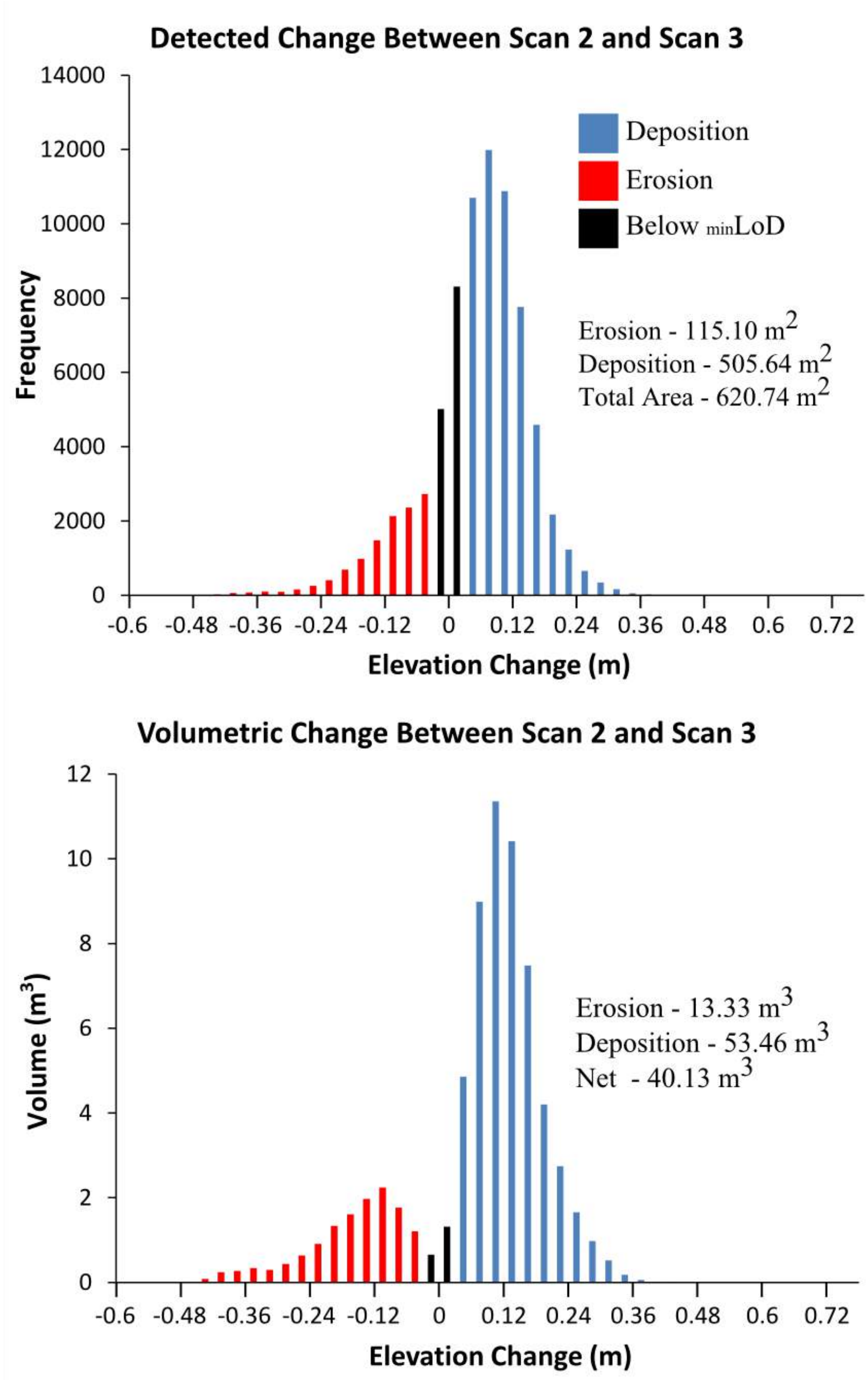

Figure 5.9: Histograms displaying cell frequency and volumetric distribution of DoD 2. Positive blue values indicate deposition and negative red values indicate erosion. Values below the 0.03 m threshold are shown in black. Written values refer to thresholded DoD.

	Thresholded DEM of Difference	DoD 1	DoD 2
Areal	**Total Area of Erosion (m^2)**	443.77	115.10
	Total Area of Deposition (m^2)	187.95	506.64
	Total Area of Detectable Change (m^2)	631.72	620.74
	Percent of Area of Interest with Detectable Change	89.18%	82.33%
Volumetric	**Total Volume of Erosion (m^3)**	88.53	13.33
	Total Volume of Deposition (m^3)	39.12	53.46
	Total Net Volume Difference (m^3)	-49.40	40.13
Vertical Averages	**Average Depth of Erosion (m)**	0.20	0.12
	Average Depth of Deposition (m)	0.21	0.11
Percentage (by volume)	**Percent Erosion**	69.23%	19.96%
	Percent Deposition	30.77%	80.04%

Table 5.5: Summary of both DoD analyses.

5.5 Cross Sections

Cross sections of the scan 1 and scan 2 surfaces (Figure 5.10) as well as the scan 2 and scan 3 surfaces (Figure 5.11) were created to show the magnitude of erosion and deposition along the point bar surface. Figure 5.10 shows significant erosion over most of the bar surface. As you move downstream, there is an increasing amount of deposition in the chute channel as well as on the downstream side of the point bar. Figure 5.11 shows the opposite trend, with deposition dominant over most of the bar surface and some erosion in the chute channel as well as on the downstream side of the point bar.

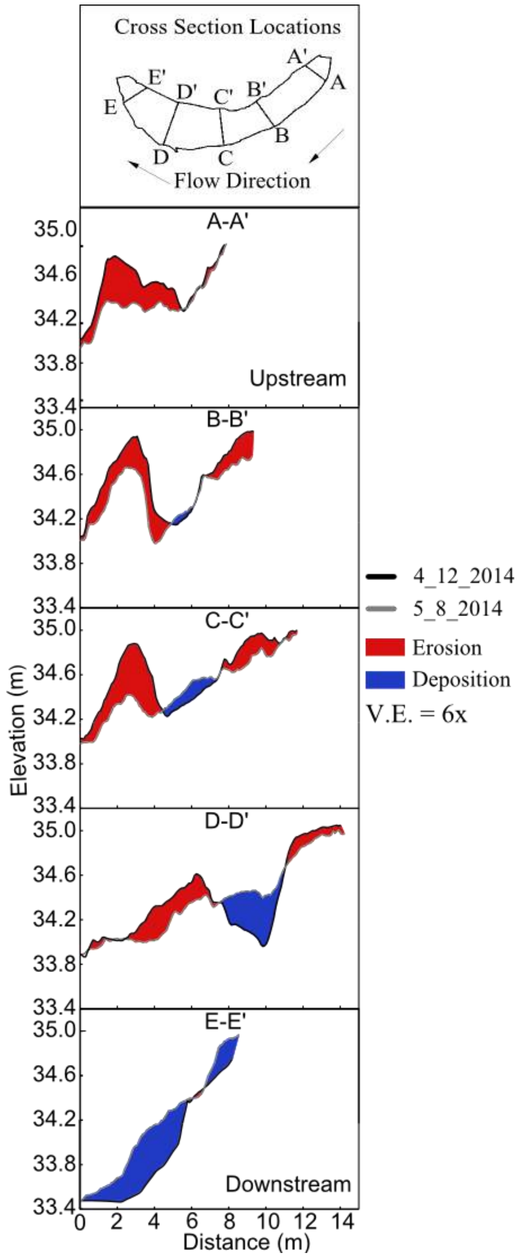

Figure 5.10: Cross sections showing elevation difference between scan 1 and scan 2. Blue indicates deposition and red indicates erosion.

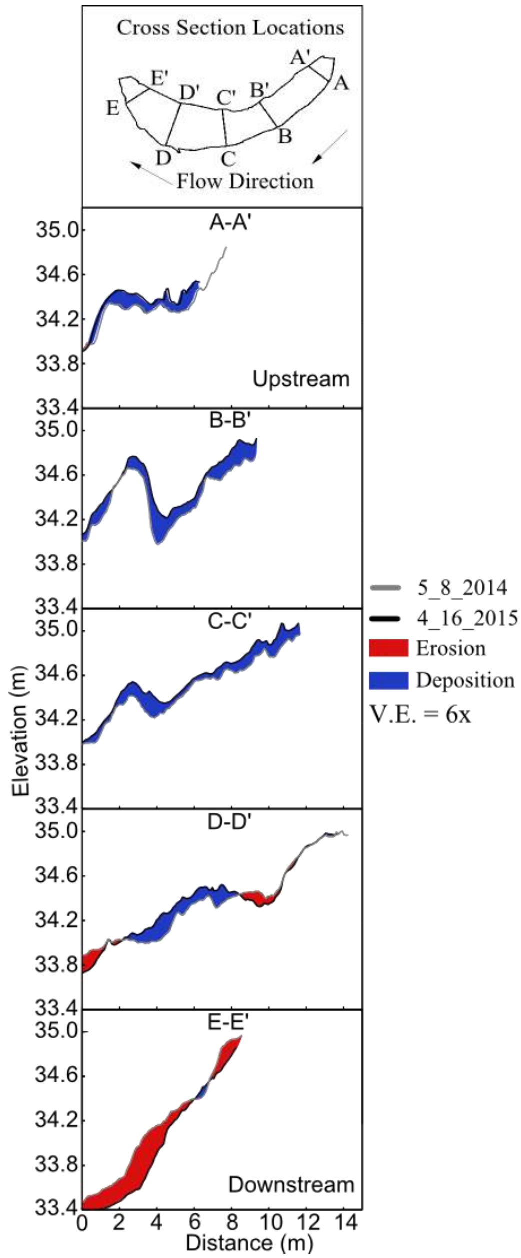

Figure 5.11: Cross sections showing elevation difference between scan 2 and scan 3. Blue indicates deposition and red indicates erosion.

5.6 Grain Size Analysis

The grain size of sediment on the point bar after the flood event on April 30, 2014 ranged from mud to cobbles (Figure 5.12). On the upstream end of the point bar, there were ridges of muddy sand up to 20 m in length and 0.10 m high. In this area, there were patches composed of sand, and other patches composed of sand and gravel mixtures. Along the trough of the point bar, there was a large amount of sand and gravel, and a few places are dominated by cobble-sized gravel. Within the trough small lee dunes (Moody and Meade, 2014) have formed. These dunes are composed of sand and extend downstream behind vegetation patches. Two such deposits are shown within the trough in Figure 5.12. Sand and gravel were also exposed at the water's edge. The gravel here was finer than at other locations on the point bar, ranging from granules to pebbles. The scroll bar that remained after the flood event consisted mainly of sand with gravel scattered throughout. Much of the downstream end of the bar had a thick layer of well sorted coarse sand that was deposited from the storm event. This sand was also present in thick deposits up on the flood plain outside the scanned area.

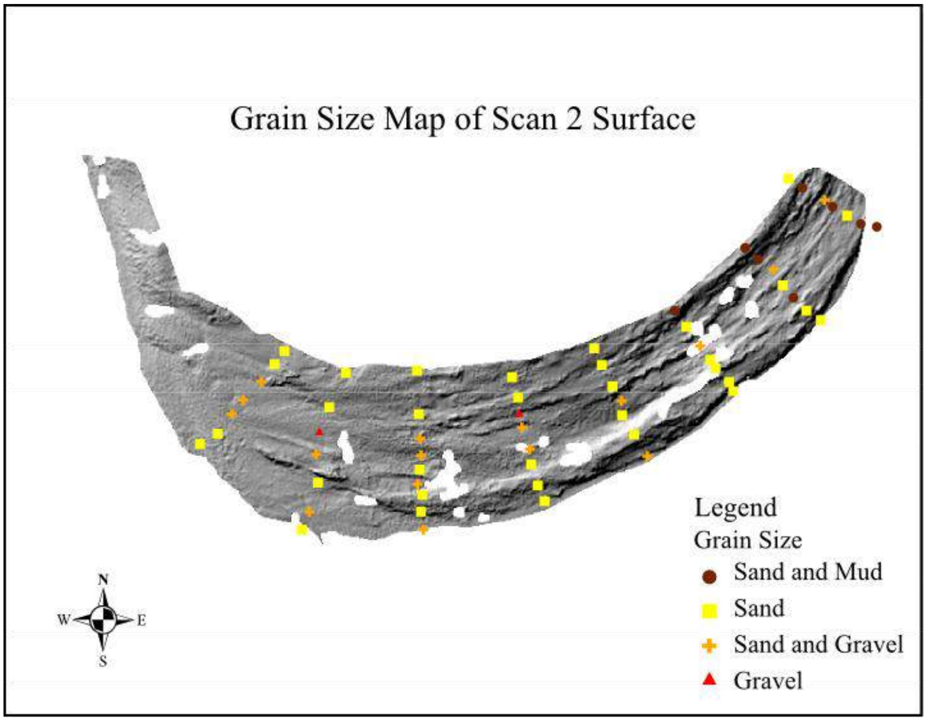

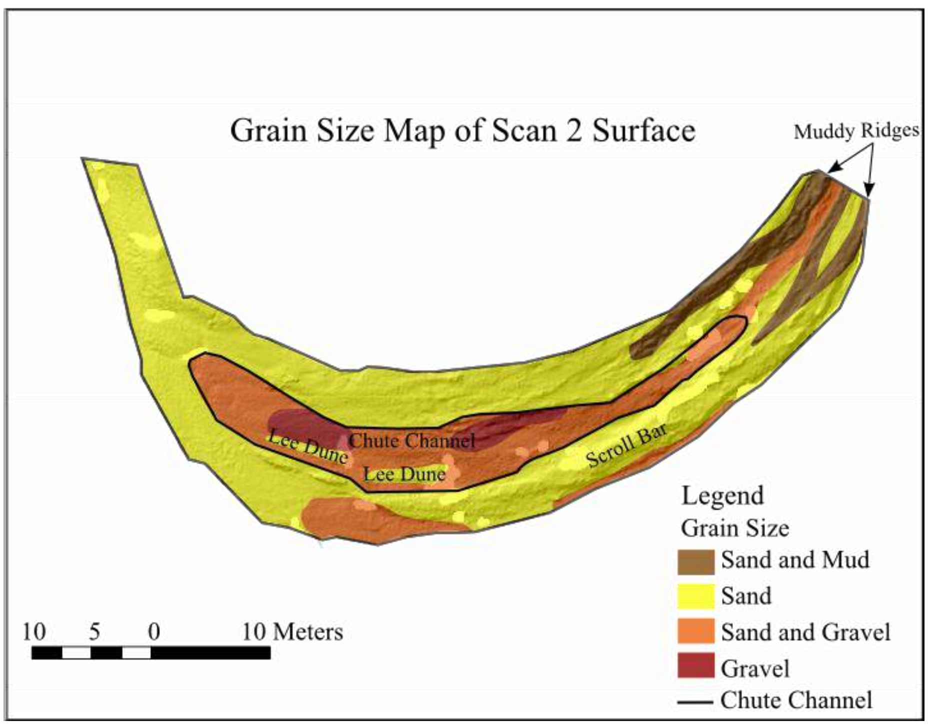

Figure 5.12: The top image shows hillshade of the scan 2 area with the location and description of each survey point. The bottom image shows the interpolated grain size map of the scan 2 surface.

Chapter 6

DISCUSSION

The 6.1 year flood caused a significant amount of erosion to the point bar. Before the event, the point bar consisted of a well-developed scroll bar, as well as a relatively deep (0.50 m) chute channel. Sediment on the upstream end of the point bar consisted of gravel and transitioned to sand on the downstream end of the bar. The sediment at the base of the chute channel consisted of sand and gravel with patches of coble-sized material. The scroll bar was vegetated and consisted mainly of sand and muddy sand. The downstream end of the point bar had a steep embankment and the point bar came to an abrupt end where it joined with the upper floodplain surface.

After the flood, significant erosion occurred to the scroll bar. In places, over 0.70 m of sediment was removed. Additionally, the chute channel filled in up to 0.60 m, especially on the downstream end of the point bar. The point bar itself was extended by about 2.0 m into the channel near cross section E – E'. The majority of deposits were coarse sand that extended the point bar and coarse sand and gravel that filled in the chute channel. Overall, the point bar experienced net erosion, which accounted for 69% of the area that had detectable change. The irregular shape seen in the first scan was flattened due to scour and fill. While point bars are considered depositional features, we can infer from these results that moderate size flood events can cause a net loss in point bar volume.

Figure 5.12 shows the grain size map of the point bar surface after the 6.1 year flood. We can see that there are two distinct deposits of sand in the chute channel. These deposits are lee dunes, first described by Moody and Meade (2008). Upstream of each of the deposits was a patch of vegetation. This can be seen in Figure 5.12 and in the Figure 5.4, where patches of vegetation in the point cloud and resulting DEM were cut out. We can infer that these deposits form during high flow when water is diverted around objects and sediment is deposited in the lee of them.

The smaller high flow events that occurred between scan 2 and scan 3 resulted in net deposition on the point bar and the re-growth of some of the features we originally saw in scan 1. Grain size remained similar between scan 2 and scan 3, but the dominant material that was transported was sand and mud. It is likely that these small events were not able to transport gravel on the bar surface. The most significant result we observed was the redevelopment of the scroll bar. Around 80% of the point bar experienced net erosion, with the highest deposition occurring on the scroll bar and in the chute channel. It appears that the scroll bar grew both vertically and laterally landward. Our results are in agreement with Moody and Meade (2014) who found landward growth of the scroll bar and stratigraphic evidence of erosion and deposition preserved in scroll bar deposits. Erosion was dominant on the downstream end of the point bar. It appears that much of the sediment that was deposited on the downstream end of the point bar after the 6.1 year flood had been removed by these smaller events, or during normal flow conditions.

Both DoD analyses showed very little erosion to the chute channel. In fact, most of the chute channel experienced net deposition. There were a few places within each DoD where scour holes developed within the chute channel. This leads us to believe that chute channels may not always form during high flow. These results are consistent with Kasvi et al. (2012), who observed the effects of high flow events on two point bars and found no chute channel formation. Other features, such as head-cut gullies may need to form first to promote the formation of a chute channel. An alternative explanation is that the chute channel is a remnant of the original point bar platform, and once the scroll bar forms; it appears that there is a chute channel when in actuality there has been no significant scour. Moody and Meade (2014) documented the formation of a chute channel through the deposition of a confining bank that created a secondary scroll bar. This secondary ridge promoted the erosion of the chute channel in the low area between the two scroll bars.

An important aspect of this study was to gain a better understand of the amount of sediment that is exchanged between point bar deposits and the river. This is necessary for calculating sediment budgets and determining transit time distributions of sediment stored in point bars. Given that point bars are depositional features, we would expect to see deposition under normal flow conditions. Between scan 2 and scan 3 we observed this trend and saw overall accretion on the point bar. Between scan 1 and scan 2, where we had a high flow velocity and discharge, we saw significant erosion. This suggests that in a normal year with no large flood events, we would expect the point bar to gain approximately 40 m^3 of sediment. In addition, we would expect the point bar to lose approximately 50 m^3 of sediment with events of similar magnitude to the 6.1 year flood. What is uncertain is where the transition is from deposition to erosion. If the 2 year flood causes net erosion, than sediment residence time on the active point bar will be short.

Additionally, our results show that it is important to monitor morphological features after every high flow event. If only annual surveys were completed, we would have missed much of the erosion that occurred as a result of the 6.1 year flood. Throughout most of the year, there is too much vegetation on the point bar to obtain the coverage needed to create a high resolution DEM. This would limit our ability to determine the geomorphic change that occurs from every flood event.

Chapter 7

CONCLUSIONS

Our study shows that TLS is an effective tool for monitoring areal, volumetric, and geomorphic changes to point bars. With a growing interest in understanding small-scale geologic features such as point bars, riverbanks, and landslides, there is a need to better develop TLS processing methodologies. The methods presented in this thesis produce highly accurate models that allow us to understand small geomorphic features better than traditional survey techniques. Techniques such as total station surveys rely on very few points, and their volumetric calculations result in a high amount of uncertainty. With TLS point clouds and their resulting DEMs there is much less uncertainty due to improved coverage and point density, as well as less interpolation.

Based on our results of 3 TLS surveys, we were able to document the effects that small and moderate sized flow events have on a typical point bar of the White Clay Creek. Moderate sized events caused net erosion to the point bar surface and can also extend the point bar downstream. The scroll bar experienced significant erosion, while the chute channel was filled in. Additionally, we were able to observe the formation of lee dunes formed behind patches of vegetation. Smaller, more frequent events inundate the point bar and cause net deposition. These events have lower flow velocities and discharge, which promote point bar formation and growth. The scroll bar accreted both vertically and landward, while the chute channel continued to fill, in most places.

While deposition is the dominant process controlling the growth of point bars, we found that erosion has a significant effect on their evolution. In order to interpret the geologic history of floodplain deposits preserved in the rock record, quantitative estimates of erosion and deposition need to be completed. While this thesis was not concerned with the stratigraphy of point bar deposits, we believe that our results will add to the existing knowledge on how their deposits are preserved. Furthermore, continued monitoring of the site will allow additional erosional and depositional estimates to be quantified after flood events of varying sizes. This will allow for a transit time distribution of active point bar sediments to be calculated.

REFERENCES

Allmendinger, N. E., Pizzuto, J. E., Moglen, G. E., & Lewicki, M. (2007). A sediment budget for an urbanizing watershed, 1951-1996, Montgomery County, Maryland, USA 1. *JAWRA Journal of the American Water Resources Association*, *43*(6), 1483-1498.

Allmendinger, N. E., Pizzuto, J. E., Potter, N., Johnson, T. E., & Hession, W. C. (2005). The influence of riparian vegetation on stream width, eastern Pennsylvania, USA. *Geological Society of America Bulletin*, *117*(1-2), 229-243.

Allmendinger, N.E. (2004). The influence of convex-bank floodplains on stream channel processes and morphology in the Mid-Atlantic Piedmont. Ph.D Thesis, University of Delaware, Newark, Delaware, 223 pp.

Bain, D. J. & Brush, G. S. (2005). Early chromite mining and agricultural clearance: Opportunities for the investigation of agricultural sediment dynamics in the eastern piedmont (USA). *American Journal of Science*, *305*(9), 957-981.

Bolin, B. & Rodhe, H. (1973). A note on the concepts of age distribution and transit time in natural reservoirs. *Tellus*, *25*(1), 58-62.

Bradley, D. N., & Tucker, G. E. (2013). The storage time, age, and erosion hazard of laterally accreted sediment on the floodplain of a simulated meandering river. *Journal of Geophysical Research: Earth Surface*, *118*(3), 1308-1319.

Brierley, G.J. & Fryirs, K.A. (2005). *Geomorphology and river management: Applications of the river styles framework*. Blackwell Publications.

Brodu, N. & Lague, D. (2012). 3D terrestrial LiDAR data classification of complex natural scenes using a multi-scale dimensionality criterion: Applications in geomorphology. *ISPRS Journal of Photogrammetry and Remote Sensing*, *68*, 121-134.

CloudCompare (2014) (version 2.6) [GPL Software]. EDF R&D, Telecom ParisTech. Retrieved from http://www.cloudcompare.org/.

Delaware Climate Information. (2010). Retrieved June 4, 2015, from http://climate.udel.edu/delawares-climate

Eriksson, E. (1971), Compartment models and reservoir theory. *Annual Review of Ecology and Systematics 2*, 67-84.

Fryirs, K.A. & Brierley, G.J. (2013). *Geomorphic analysis of river systems: An approach to reading the landscape.* John Wiley and Sons.

Ghinassi, M. (2011). Chute channels in the Holocene high-sinuosity river deposits of the Firenze plain, Tuscany, Italy. *Sedimentology*, *58*(3), 618-642.

Jacobson, R. B. & Coleman, D. J. (1986). Stratigraphy and recent evolution of Maryland Piedmont flood plains. *American Journal of Science*, *286*(8), 617-637.

Kane, R. (2015). Using terrestrial laser scanning for differential measurement of interannual rock glacier movement in the Argentine dry Andes. MS Thesis, University of Delaware, Newark, Delaware, 52 pp.

Kasvi, E., Vaaja, M., Alho, P., Hyyppä, H., Hyyppä, J., Kaartinen, H., & Kukko, A. (2013). Morphological changes on meander point bars associated with flow structure at different discharges. *Earth Surface Processes and Landforms*, *38*(6), 577-590.

Kuo, C. W., Brierley, G., & Chang, Y. H. (2015). Monitoring channel responses to flood events of low to moderate magnitudes in a bedrock-dominated river using morphological budgeting by terrestrial laser scanning. *Geomorphology*, *235*, 1-14.

Moody, J. A. & Meade, R. H. (2008). Terrace aggradation during the 1978 flood on Powder River, Montana, USA. *Geomorphology*, *99*(1), 387-403.

Moody, J. A. & Meade, R. H. (2014). Ontogeny of point bars on a river in a cold semi-arid climate. *Geological Society of America Bulletin*, *126*(9-10), 1301-1316.

Nanson, G. C. & Croke, J. C. (1992). A genetic classification of floodplains. *Geomorphology*, *4*(6), 459-486.

Nanson, G. C. (1980). Point bar and floodplain formation of the meandering Beatton River, northeastern British Columbia, Canada. *Sedimentology*, *27*(1), 3-29.

O'Neal, M. A. & Pizzuto, J. E. (2011). The rates and spatial patterns of annual riverbank erosion revealed through terrestrial laser-scanner surveys of the South River, Virginia. *Earth Surface Processes and Landforms*, *36*(5), 695-701.

Picco, L., Mao, L., Cavalli, M., Buzzi, E., Rainato, R., & Lenzi, M. A. (2013). Evaluating short-term morphological changes in a gravel-bed braided river using terrestrial laser scanner. *Geomorphology*, *201*, 323-334.

Pizzuto, J. E. & Meckelnburg, T. S. (1989). Evaluation of a linear bank erosion equation. *Water Resources Research*, *25*(5), 1005-1013.

Pizzuto, J. E., Hession, W. C., & McBride, M. (2000). Comparing gravel-bed rivers in paired urban and rural catchments of southeastern Pennsylvania. *Geology*, *28*(1), 79-82.

Schenck, W.S., Plank, M.O., Srogi, L., 2000, Bedrock Geologic Map of the Piedmont of Delaware and Adjacent Pennsylvania: Delaware Geological Survey Geologic Map 10, scale 1:36,000

Skalak, K. & Pizzuto, J. (2010). The distribution and residence time of suspended sediment stored within the channel margins of a gravel-bed bedrock river. *Earth Surface Processes and Landforms*, *35*(4), 435-446.

Starek, M. J., Mitásova, H., Wegmann, K. W., & Lyons, N. (2013). Space-time cube representation of stream bank evolution mapped by terrestrial laser scanning. *Geoscience and Remote Sensing Letters, IEEE*, *10*(6), 1369-1373.

United States Water Resources Council. (1981). *Guidelines for determining flood flow frequency* (Bulletin No. 17B). Washington, DC.

Walter, R. C. & Merritts, D. J. (2008). Natural streams and the legacy of water-powered mills. *Science, 319*(5861), 299-304.

Wheaton, J. M., Brasington, J., Darby, S. E., & Sear, D. A. (2010). Accounting for uncertainty in DEMs from repeat topographic surveys: improved sediment budgets. *Earth Surface Processes and Landforms*, *35*(2), 136-156.

Wolman, M. G. & Leopold, L. B. (1957). River flood plains; some observations on their formation (No. 282-C).

Wolman, M. G. (1967). A cycle of sedimentation and erosion in urban river channels. *Geografiska Annaler. Series A. Physical Geography*, 385-395.

Appendix

SUPPLEMENTAL MATERIAL

Figure A.1: Site Photos.

April 11, 2014 surface, looking downstream.

May 8, 2014 surface, looking downstream.

April 16, 2015 surface, looking upstream.

March 22, 2015 surface, looking downstream (left) and upstream (right). The March 22 surface is a good representative of the April 16 surface.

Figure A.2: Co-Registered point clouds of Scan 1(a), Scan 2(b), and Scan 3(c).

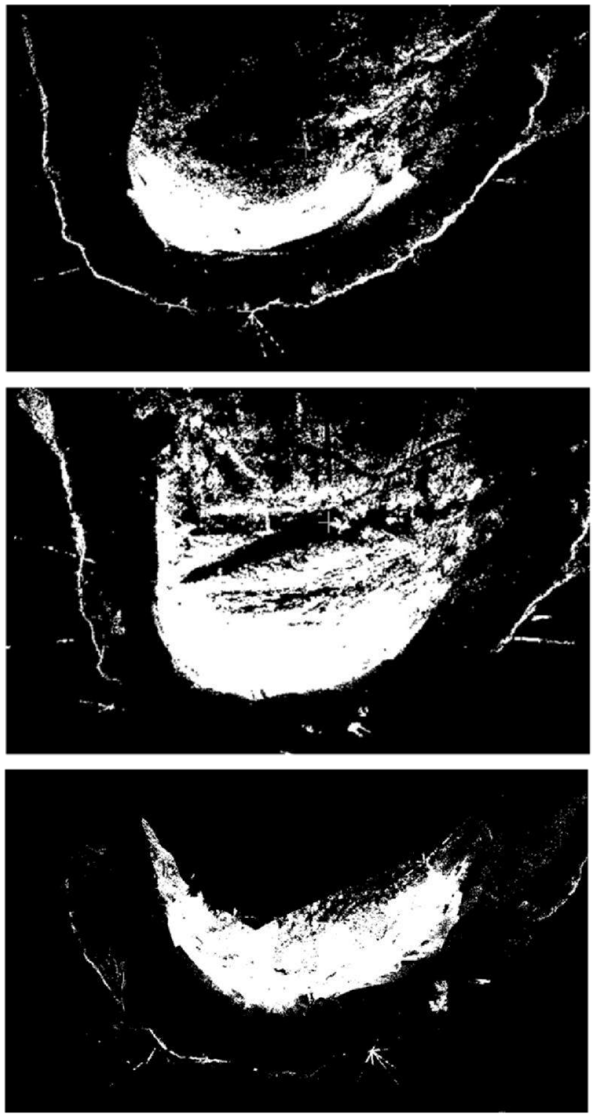

a.)
b.)
c.)

Figure A.3: Regional Skew Map

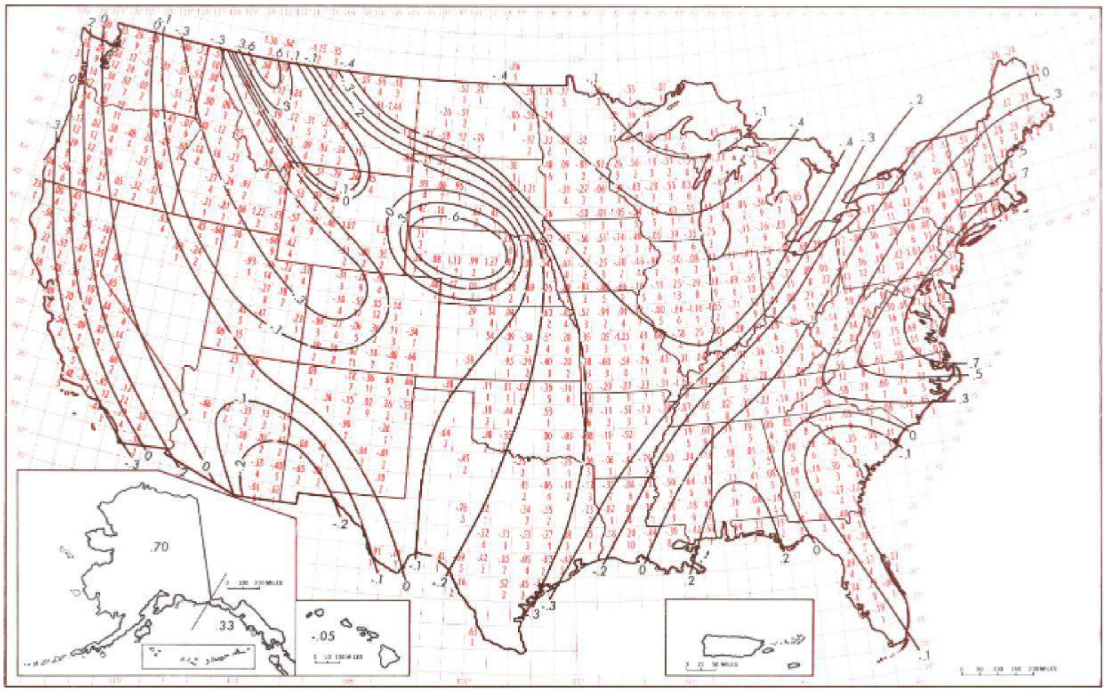

GENERALIZED SKEW COEFFICIENTS OF LOGARITHMS OF ANNUAL MAXIMUM STREAMFLOW

AVERAGE SKEW COEFFICIENT BY ONE DEGREE QUADRANGLES

Lower number in each quadrangle is number of stream gaging stations for which the average shown above it was computed

Figure A.4: Survey data for grain size analysis and benchmark locations relative to benchmark 1.

X (m)	Y (m)	Z (m)	Description
0	0	0	BM1
0	41.248	0.378	BM2
23.51	-24.99	0.553	BM3
3.295	81.046	0.855	BM4
4.394	49.836	-1.135	SM
3.79	48.607	-0.753	SM
2.784	47.697	-0.734	S
1.728	46.726	-0.615	S
1.013	46.223	-0.525	SG
-0.452	44.713	-0.222	SM
-1.551	43.787	0.141	SM
10.664	43.13	-1.126	S
9.548	42.185	-0.7	S
8.212	41.427	-0.701	SM
6.957	40.842	-0.702	S
5.454	40.456	-0.629	SG
4.278	39.473	-0.505	SM
3.048	38.678	0.032	SM
14.361	34.358	-1.111	S
13.545	34.247	-0.731	S
12.106	33.475	-0.456	S
11.322	33.241	-0.609	S
9.957	32.745	-0.774	SG
8.094	32.057	-0.459	S
6.496	31.488	-0.072	SM
17.654	25.898	-1.137	GS
15.631	25.316	-0.522	S
13.746	24.801	-1.077	S
12.558	25.079	-0.913	SG
11.206	24.678	-0.504	S
9.214	24.32	-0.281	S

Continued:

X (M)	Y (M)	Z (M)	Description
18.927	16.5	-1.141	S
16.854	16.041	-0.626	S
15.635	16.265	-0.789	S
14.354	16.512	-0.666	SG
12.404	16.374	-0.586	SG
11.19	16.509	-0.477	G
9.897	16.769	-0.138	S
8.107	16.741	0.054	S
18.367	6.015	-1.132	GS
16.91	6.237	-1.027	S
15.574	6.726	-0.644	S
14.587	6.603	-0.842	SG
13.443	7.109	-0.719	S
12.322	7.562	-0.719	SG
10.965	7.85	-0.405	GS
8.954	8.328	-0.219	S
5.388	9.177	0.267	S
15.608	-3.848	-1.18	S
14.321	-2.817	-0.99	GS
12.139	-1.445	-0.979	S
9.8	-0.936	-0.503	SG
7.995	-0.142	-0.469	G
6.284	1.218	-0.453	S
3.909	3.359	0.154	S
6.249	-10.136	-1.146	S
5.851	-8.454	-0.904	S
4.574	-6.84	-0.757	GS
3.701	-5.611	-0.44	GS
2.665	-3.692	-0.395	GS
1.514	-2.229	-0.116	S
0.713	-1.106	0.102	S

BM = Benchmark, SM = Sand and Mud, S = Sand, SG = Sand and Gravel, G = Gravel

Figure A.5: TIN Models created from point cloud data.